Journal of Molecular and Cellular Cardiology 74 (2014) 115–124

Contents lists available at ScienceDirect

Journal of Molecular and Cellular Cardiology

journal homepage: www.elsevier.com/locate/yjmcc

Original article

Calmodulin mutations associated with long QT syndrome prevent inactivation of cardiac L-type Ca^{2+} currents and promote proarrhythmic behavior in ventricular myocytes

Worawan B. Limpitikul [a,1], Ivy E. Dick [a,1], Rosy Joshi-Mukherjee [a], Michael T. Overgaard [c], Alfred L. George Jr. [d,e,2], David T. Yue [a,b,*]

[a] Calcium Signals Laboratory, Department of Biomedical Engineering, The Johns Hopkins University School of Medicine, Baltimore, MD 21205
[b] Department of Neuroscience, The Johns Hopkins University School of Medicine, Baltimore, MD 21205
[c] Department of Biotechnology, Chemistry and Environmental Engineering, Aalborg University, Denmark
[d] Department of Medicine, Vanderbilt University, Nashville, TN 37232, USA
[e] Department of Pharmacology, Vanderbilt University, Nashville, TN 37232, USA

ARTICLE INFO

Article history:
Received 11 April 2014
Accepted 28 April 2014
Available online 8 May 2014

Keywords:
Calmodulin
Ca^{2+}/CaM-dependent inactivation (CDI)
L-type Ca^{2+} channel
Long-QT syndrome
APD prolongation

ABSTRACT

Recent work has identified missense mutations in calmodulin (CaM) that are associated with severe early-onset long-QT syndrome (LQTS), leading to the proposition that altered CaM function may contribute to the molecular etiology of this subset of LQTS. To date, however, no experimental evidence has established these mutations as directly causative of LQTS substrates, nor have the molecular targets of CaM mutants been identified. Here, therefore, we test whether expression of CaM mutants in adult guinea-pig ventricular myocytes (aGPVM) induces action-potential prolongation, and whether affiliated alterations in the Ca^{2+} regulation of L-type Ca^{2+} channels (LTCC) might contribute to such prolongation. In particular, we first overexpressed CaM mutants in aGPVMs, and observed both increased action potential duration (APD) and heightened Ca^{2+} transients. Next, we demonstrated that all LQTS CaM mutants have the potential to strongly suppress Ca^{2+}/CaM-dependent inactivation (CDI) of LTCCs, whether channels were heterologously expressed in HEK293 cells, or present in native form within myocytes. This attenuation of CDI is predicted to promote action-potential prolongation and boost Ca^{2+} influx. Finally, we demonstrated how a small fraction of LQTS CaM mutants (as in heterozygous patients) would nonetheless suffice to substantially diminish CDI, and derange electrical and Ca^{2+} profiles. In all, these results highlight LTCCs as a molecular locus for understanding and treating CaM-related LQTS in this group of patients.

1. Introduction

Calmodulin (CaM) is a ubiquitous Ca^{2+}-sensor molecule that modulates a vast array of proteins, thereby controlling signaling cascades via Ca^{2+}-dependent adjustment of relevant proteins. As such, CaM critically orchestrates numerous functions, including cellular excitability, muscle contraction, memory, and immunological responses [1,2]. So important are the functions of CaM that it has long been thought that naturally occurring mutations within this molecule would prove lethal, and that such mutations would thereby play little role in disease processes afflicting living individuals.

Yet, a role for CaM in a number of diseases has begun to emerge. Alterations in the overall level of CaM have been implicated in heart failure [3], schizophrenia [4], and Parkinson's disease [5–7]. Outright CaM mutations in *Drosophila* have been associated with muscle malfunction [8]. Very recently, human genetic studies uncovered *de novo* and heritable CaM mutations (N54I and N98S, start methionine denoted residue 1) that are associated with 11 cases of catecholaminergic polymorphic ventricular tachycardia (CPVT), where altered CaM-ryanodine receptor function is implicated as a major contributing factor [9]. Further, whole-exome sequencing and targeted gene sequencing have revealed an association between three *de novo* missense CaM mutations and severe long-QT syndrome (LQTS) with recurrent cardiac arrest [10]. The first hints of underlying mechanism can be gleaned by relating the locations of these mutations to the basic structure–function layout of CaM, a 17 kDa protein comprised of N- and C-terminal lobes linked by a flexible helix. Each lobe of CaM contains two EF hands, canonical Ca^{2+} binding

Abbreviations: CaM, calmodulin; CPVT, catecholaminergic polymorphic ventricular tachycardia; LQT(S), long-QT (syndrome); aGPVM(s), adult guinea-pig ventricular myocyte(s); LTCC(s), L-type Ca^{2+} channels; apoCaM, Ca^{2+}-free calmodulin; APD, action potential duration; CDI, Ca^{2+}/CaM-dependent inactivation.

* Corresponding author at: Calcium Signals Laboratory, Department of Biomedical Engineering, The Johns Hopkins University School of Medicine, Baltimore, MD 21205. Tel.: +1 410 955 0078; fax: +1 410 955 0549.
E-mail address: dyue@jhmi.edu (D.T. Yue).
[1] Tel.: +1 410 955 0078; fax: +1 410 955 0549.
[2] Present address: Department of Pharmacology, Northwestern University Feinberg School of Medicine, Chicago, IL 60611, USA.

http://dx.doi.org/10.1016/j.yjmcc.2014.04.022
0022-2828/

motifs, with the N-lobe having slightly lower Ca^{2+} binding affinity. Ca^{2+} binding to these EF hands induces a conformational change that alters function of target molecules to which CaM is bound, thus transducing changes of intracellular Ca^{2+} concentration [11] into modulation of molecular function. Each of the LQTS mutations (D96V, D130G, and F142L, with start methionine denoted residue 1) resides at or near Ca^{2+} coordinating residues within the EF hands of the C-lobe of CaM, and have been shown to decrease affinity for Ca^{2+} binding [10]. By contrast, the reported CPVT mutations in CaM imparted little-to-mild reduction of Ca^{2+} binding affinity [9]. It is perhaps interesting to speculate that the contrasting effects on Ca^{2+} binding may underlie the elaboration of distinguishable LQTS and CPVT phenotypes by these two classes of mutations. At present, however, the mechanisms linking these mutations in CaM to their corresponding disease phenotypes are essentially unknown.

That said, progress towards elucidating these mechanisms will ultimately prove invaluable in devising personalized therapeutics for afflicted individuals, and in gleaning general lessons about LQTS pathogenesis from these single-point-mutation case examples. Among the most prominent mechanistic unknowns are the following. First, do the LQTS CaM mutations actually cause the emergence of LQTS substrates in heart? At present, no experimental evidence directly establishes causality. Second, what are the predominant molecular targets through which CaM mutations exert their actions in heart? Likely cardiac myocyte targets abound, including ryanodine receptors (RyR2), voltage-gated Na channels ($Na_V1.5$), slowly activating delayed-rectifier K channels (I_{Ks}), and L-type Ca^{2+} channels [10–12] ($Ca_V1.2$). All of these contribute to shaping action-potential morphology and thereby represent plausible candidates. Third, the severity of the LQTS fits in a seemingly incongruous fashion with the redundancy of human CaM genes (*CALM1*, *CALM2*, and *CALM3*), each of which encodes for an identical CaM molecule at the protein level. Given the heterozygosity of these LQTS patients [10], this redundancy implies that only one of six alleles of CaM would possess a mutation, yielding only a portion of mutant versus wild-type CaM.

Here, therefore, we acutely introduce LQTS CaM mutants into adult guinea-pig ventricular myocytes (aGPVMs) and demonstrate marked prolongation of action potentials, along with intense disturbance of Ca^{2+} cycling. As these effects are reminiscent of those we observed previously by man-made CaM mutants acting strongly through diminished CaM-mediated regulation of L-type Ca^{2+} channels [13] (LTCCs), we tested directly for the effects of naturally occurring LQTS CaM mutants on these very channels. Indeed, we establish that Ca^{2+} regulation of LTCCs can be strongly suppressed by overexpression of LQTS CaM mutants, posturing altered regulation of these channels as an important contributor to the LQTS phenotype. By contrast, overexpressing CPVT CaM mutants caused weaker or undetectable perturbation of LTCC function and action potentials. Finally, we note the requirement that a single Ca^{2+}-free CaM (apoCaM) must first preassociate with LTCCs for subsequent Ca^{2+} regulation to occur [5,11,14–17], and substantiate how this feature rationalizes how a limited fraction of LQTS CaM mutants can nonetheless elaborate significant perturbation of channel regulation, sufficient to appreciably prolong action potentials.

2. Methods

2.1. Adult guinea-pig ventricular myocyte isolation and adenoviral transduction

Adult guinea-pig ventricular myocytes (aGPVMs) were isolated from whole hearts of adult guinea pigs (Hartley strain, 3–4 wk old, weight 250–350 g). Hearts were excised after guinea pigs were anesthetized with pentobarbital (35 mg/kg, intraperitoneal injection). Single ventricular myocytes were isolated from both ventricles according to a published protocol [18] and plated on glass coverslips coated with laminin (20 μg/ml overnight at 4 °C). Cells were transduced with adenovirus carrying wild-type or mutant CaM upon plating in the presence of M199 medium supplemented with 20% fetal bovine serum. Expression of wild-type CaM had little effect on action-potential morphology or duration, as compared to uninfected myocytes (Supplementary Fig. 1). After 4 h, the medium was replaced by M199 medium with 0% fetal bovine serum to maintain the phenotype of acutely dissociated myocytes. Cells were maintained at 37 °C and recording was done at room temperature 20–36 h later.

2.2. Molecular biology

LQTS CaM mutations were generated using QuikChange™ site-directed mutagenesis (Agilent Technologies, Inc.) on rat brain CaM (M17069) in the pcDNA3 vector (Invitrogen). CPVT CaM mutations were generated on human *CALM1* gene in the pcDNA3 vector (a kind gift from Michael T. Overgaard [9]). For electrophysiological recordings in HEK293 cells, both wild-type and LQTS mutant CaMs were cloned into the pIRES2-EGFP vector (Clontech Laboratories, Inc.) using *NheI* and *BglII*. For adenoviral expression in aGPVMs, wild-type and mutant CaMs were cloned into the pAdCiG viral shuttle vector using *XhoI* and *SpeI*. Adenovirus was amplified via a standard cre-recombinase method as previously described [13].

The human cardiac α_{1C} cDNA was constructed by cloning in an ~1.6 kbase upstream fragment of the cardiac (containing exon 8a) channel variant (kind gift from Tuck Wah Soong [19]) into a human $\alpha_{1C\text{-}1}$ backbone (NM_000719 kindly gifted from Charlie Cohen of Merck Pharmaceuticals) contained within pcDNA3.1, via *HindIII* and *ClaI* sites.

For FRET two-hybrid constructs, CaM and CI region of $Ca_V1.2$ channels (as defined in Fig. 5A and described previously [14]) were tagged on their amino termini with fluorophores (cerulean and venus, respectively) with a linker of 3 alanines, and cloned into the pcDNA3.0 (Invitrogen) using *KpnI* and *XbaI*.

2.3. Transfection of HEK293 cells

For whole-cell patch clamp experiments, HEK293 cells were cultured on glass coverslips in 10-cm dishes and Ca^{2+} channels were transiently transfected using a standard calcium phosphate method [20]. 8 μg of human cardiac α_{1C} cDNA (as described above) was co-expressed heterologously with 8 μg of rat brain β_{2a} (M80545), 8 μg of rat brain $\alpha_2\delta$ (NM_012919.2) subunits, and 8 μg of wild-type or mutant CaMs, except for mixing experiments (Fig. 6) where various molar ratios of wild-type to mutant CaM were transfected. The auxiliary β_{2a} subunit was chosen so as to minimize the confounding effects of voltage-dependent inactivation on Ca^{2+}/CaM-dependent inactivation [21]. To increase expression levels, 2 μg of simian virus 40 T antigen cDNA was co-transfected. Expression of all constructs was driven by a cytomegalovirus promoter.

For FRET two-hybrid experiments, HEK293 cells were cultured on glass-bottom dishes and transfected with polyethylenimine [22] (PEI) before epifluorescence imaging. Whole-cell patch clamp and FRET two-hybrid experiments were performed 1–2 days after transfection.

2.4. Electrophysiology

Whole-cell voltage-clamp recordings of HEK293 cells were done 1–2 days after transfection at room temperature. Recordings were obtained using an Axopatch 200B amplifier (Axon Instruments). Whole-cell voltage-clamp records were lowpass filtered at 2 kHz, and then digitally sampled at 10 kHz. P/8 leak subtraction was used, with series resistances of 1–2 MΩ. For voltage-clamp experiments, internal solutions contained (in mM): $CsMeSO_3$, 114; CsCl, 5; $MgCl_2$, 1; MgATP, 4; HEPES (pH 7.3), 10; and either BAPTA, 10 or EGTA, 1; at 295 mOsm adjusted with $CsMeSO_3$. The free Ca^{2+} concentrations in these BAPTA- and EGTA-containing were respectively estimated to be ~2.4 and 0.45 pM [23], assuming a contaminant Ca^{2+} concentration of 25 μM (standard

conversion at http://maxchelator.stanford.edu/). External solutions contained (in mM): TEA-$MeSO_3$, 140; HEPES (pH 7.4), 10; and $CaCl_2$ or $BaCl_2$, 40; at 300 mOsm, adjusted with TEA-$MeSO_3$. These solutions produced the following uncorrected junction potentials: 10 BAPTA/40 Ca^{2+}: 10.5 mV; 10 BAPTA/40 Ba^{2+}: 10.2 mV; 1 EGTA/40 Ca^{2+}: 11.4 mV; 1 EGTA/40 Ba^{2+}: 11.1 mV [24]. Fraction of peak current remaining after 300-ms depolarization (r_{300}) to various voltages was measured. The extent of Ca^{2+}/CaM-dependent inactivation (CDI) was calculated as $f_{300} = (r_{300/Ba} - r_{300/Ca})/r_{300/Ba}$.

Whole-cell recordings of aGPVMs were performed 20–36 h post isolation on the same recording setup. Internal solutions for voltage clamp experiments contained (in mM): $CsMeSO_3$, 114; CsCl, 5; $MgCl_2$, 1; MgATP, 4; HEPES (pH 7.3), 10; BAPTA, 10; and ryanodine, 0.005; at 295 mOsm adjusted with $CsMeSO_3$. External solutions contained (in mM): TEA-$MeSO_3$, 140; HEPES (pH 7.4), 10; and $CaCl_2$ or $BaCl_2$, 5; at 300 mOsm, adjusted with TEA-$MeSO_3$. These solutions produced an 8.4 mV uncorrected junction potential [24]. For current clamp, experiments, internal solutions contained (in mM): K glutamate, 130; KCl, 9; NaCl,10; $MgCl_2$, 0.5; EGTA, 0.5; MgATP, 4; and HEPES, 10 (pH 7.3 with KOH). External solution (Tyrode's solution) contained (in mM): NaCl, 135; KCl, 5.4; $CaCl_2$, 1.8; $MgCl_2$, 0.33; NaH_2PO_4, 0.33; HEPES, 5; and glucose, 5 (pH 7.4). Junction potentials for current-clamp solutions were calculated to be only 0.5 mV [24]. The time from upstroke to 80% repolarization (APD_{80}) was used as the metric for action potential duration throughout. SD_{cell}, the mean standard deviation of APD_{80} within individual cells, was used to assess the dispersion of APD_{80} at the same expression level of CaM. Throughout, whole-cell voltage-clamp records were lowpass filtered at 2 kHz, and then digitally sampled at 10 kHz. Current-clamp recordings were filtered at 5 kHz, and sampled at 25 kHz.

2.5. Ratiometric Ca^{2+} imaging

Single aGPVMs were plated on glass-bottom dishes coated with laminin. Cells were loaded with Indo-1 AM (1 μM) at room temperature for 5 min, rinsed, and further incubated for 10 min in Tyrode's solution at room temperature to allow for de-esterification of Indo-1 AM. Cells were stimulated by application of an electric field across individual cells using a Grass stimulator (SDD9) and bipolar point platinum electrodes. Recordings were made at room temperature in Tyrode's solution supplemented with 10 μM ascorbic acid [25] to buffer free radicals generated from electrical pacing and exposure to UV light. Fluorescence was measured using 340-nm excitation and 405- to 485-nm emission wavelengths. The intracellular Ca^{2+} concentration ($[Ca^{2+}]$) was calculated as $[Ca^{2+}] = K_{d/Indo} \cdot \beta \cdot (R - R_{min})/(R_{max} - R)$. R is the ratio of fluorescence signal at 405 and 485 nm. $K_{d/Indo}$ was determined as 800 nM [26]. R_{min} was determined to be 0.53 in a 0 mM Ca^{2+} Tyrode's with 5 mM EGTA and 1 μM ionomycin. R_{max} was determined to be 2.60 in a Na^+-free Tyrode's (Na^+ was replaced with choline ion to minimize the action of Na-Ca exchanger) with 10 mM Ca^{2+}, 1 μM ionomycin and 10 mM 2,3-butanedione monoxime. β, as defined by the ratio of fluorescence signal at 485 nM under Ca^{2+}-free and Ca^{2+}-bound conditions, was determined to be 2.33. Cells were stimulated with a single electrical pulse after steady-state pacing at 0.1 Hz. The total amount of Ca^{2+} entry was determined by integration of the area under Ca^{2+}-versus-time waveforms. Sarcoplasmic reticulum Ca^{2+} content (SR content) was determined by application of 5 mM caffeine to aGPVMs superfused with a Na^+-free Tyrode's (Na^+ was replaced with choline), containing 1.8 mM Ca^{2+} and 10 mM 2,3-butanedione monoxime. The concentration of caffeine was chosen to minimize Indo-1 quenching [27] but was still sufficient to empty the sarcoplasmic reticulum.

2.6. FRET two-hybrid measurement

Three-cube FRET measurements were performed on HEK293 cells cultured on glass-bottom dishes using an inverted fluorescence microscope in modified Tyrode's solution (in mM, NaCl, 138; KCl, 4; $CaCl_2$, 2; $MgCl_2$, 1; HEPES, 10; glucose, 10). FRET efficiency (E_A) of individual cells was computed based on a published protocol [15]. Differential expression of test constructs across individual cells allowed decoration of a binding curve. Effective dissociation constants ($K_{d,EFF}$) were calculated by fitting the binding curve with the equation $E_A = [D]_{free}/(K_{d,EFF} + [D]_{free}) \cdot E_{A,max}$, where $[D]_{free}$ is the free concentration of donor molecules.

2.7. Data analysis and statistics

All data were analyzed in MATLAB (The MathWorks) using custom-written scripts. For APD_{80} and Ca^{2+} transient measurements the Wilcox rank sum test was used to assess statistical significance of differences between cells expressing wild-type and mutant CaMs. In addition, variability not due to expression differences was assessed by calculating the standard deviation within each cell (SD_{cell}) for both APD_{80} and Ca^{2+} transient measurements. Statistical significance for variability was determined by a student's t-test with the Bonferroni correction for multiple samples as appropriate. Average Ca^{2+} transients are displayed ±SD. Statistical significance for SR content was assessed using a student t-test with a Bonferroni correction for multiple samples. The values are displayed as mean ± SEM. For electrophysiology and FRET two-hybrid measurements, f_{300} and E_A values were expressed as mean ± SEM, and a student's t-test was used to assess statistical significance.

3. Results

3.1. CaM mutants promote proarrhythmic electrical and Ca^{2+} activity in ventricular myocytes

CaM mutations have been associated with severe LQTS and recurrent cardiac arrest [10], but to date, no direct evidence exists that these mutations can actually promote proarrhythmic properties in an experimental cardiac model. Accordingly, before investigating specific Ca^{2+} regulatory disturbances relating to the interaction of LQTS CaM mutants and individual molecular targets, we tested whether the expression of these mutants at all perturbed the overall electrical and Ca^{2+} cycling properties of aGPVMs. This particular model was chosen because it features action potentials with a prominent plateau phase reminiscent of that in humans, making this system particularly suitable for understanding long-QT phenomena.

Fig. 1A displays the prototypic action potentials of a single such myocyte expressing only wild-type CaM (CaM_{WT}), obtained at 0.5-Hz stimulation under whole-cell current clamp. The timing of current injection stimuli is shown underneath for orientation. The waveforms are nearly identical from one stimulus to the next, with a mean action potential duration (APD_{80}) of ~300 ms [13]. Population behavior for APD_{80} is summarized in Fig. 1B, which plots the cumulative distribution of durations drawn from 285 responses in 10 cells, where P_{APD} is the probability that APD_{80} is less than the value on the abscissa. The sharp rise of the distribution confirms a mean duration of 349.6 ms, with a modest standard deviation of 79.6 ms. Additionally, the mean standard deviation of APDs within individual myocytes (SD_{cell}, intra-cell standard deviation) was only 21 ms, further indicating relatively homogeneous behavior. By contrast, adenoviral-mediated expression of CaM_{D96V} induced a strikingly different profile (Fig. 1C). Here, action potentials could be enormously elongated (red), exceeding even the interstimulus interval of 2 s. For reference, the control waveform with only CaM_{WT} present is reproduced in gray. Population data, displayed in cumulative histogram format (Fig. 1D), reveal marked lengthening and dispersion of APD_{80} values (red), with mean and standard-deviation values of 897.3 and 222.9 ms ($P < 0.001$). Here, SD_{cell} increased to 156.3 ms, indicating significant variability within each cell as compared to CaM_{WT} ($P < 0.01$). Both of these features furnish the cellular substrates

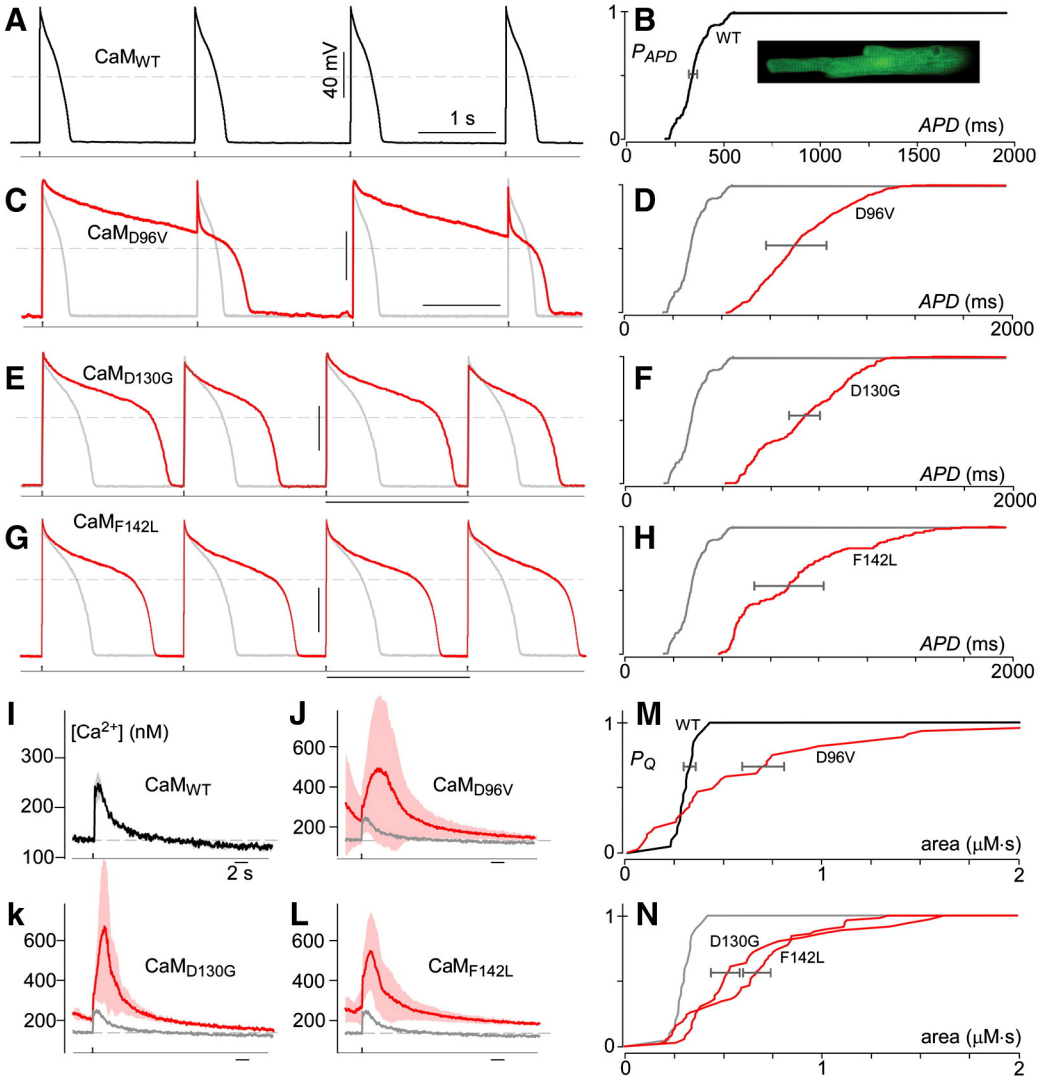

Fig. 1. CaM mutants induce arrhythmia. A, Exemplar action potentials recorded via current clamp from one-day-old aGPVMs transduced with CaM_{WT}. The stimulus waveform is depicted below. The dashed horizontal gray line indicates 0 mV, here and throughout. B, Population data corresponding to A plotted as the cumulative distribution of APD_{80} (285 responses from 10 cells). All APD_{80} population data in panels B, D, F, and H from myocytes stimulated at 0.5 Hz. Gray bar in B displays SD_{cell}. Inset shows confocal image of typical myocyte expressing GFP as a marker of transduction by adenoviral CaM_{WT}. C, Transduction of the mutant CaM_{D96V} induced marked prolongation of action potentials in this exemplar recording (red) as compared to CaM_{WT} transduction (gray, reproduced from A). D, The cumulative distribution for APD_{80} from CaM_{D96V} transduced aGPVMs (red) demonstrates a dramatic increase in APD_{80} and much greater APD_{80} variability (gray bar, $P \leq 0.01$), both as compared to myocytes transduced with CaM_{WT}. E–H, Similar AP disturbances were induced via transduction of CaM_{D130G} (E, F) and CaM_{F142L} (G, H). Example of electrical alternans in aGPVM expressing CaM_{D130G} (E). Data displayed in E and G were obtained during pacing at 1 Hz. I, Average Ca^{2+} transient (black) recorded from aGPVMs transduced with CaM_{WT} after steady-state pacing at 0.1 Hz, $n = 5$ cells. Standard deviation range shown as gray shading. Indo-1 AM was used as the inorganic Ca^{2+}-sensitive fluorescent dye. J–L, Transduction of mutant CaMs resulted in dramatic increases in the amplitude and variability of the Ca^{2+} transients. Solid gray trace reproduces the CaM_{WT} data for reference, while red and rose depict average and standard deviation of Ca^{2+} transients from aGPVMs expressing the three mutants as labeled. Data averaged from $n = 11$, 9, and 15 myocytes for respective panels J–L. M, Population data for CaM_{WT} (black) and CaM_{D96V} (red), plotted as cumulative histograms for the area integrated under the Ca^{2+} transient waveform recorded from each myocyte. Horizontal error bars depict average standard deviation of Ca^{2+} entry for transients within the same cells, and is significantly larger for each LQTS CaM mutant ($P < 0.05$). The significant right shift due to transduction of CaM_{D96V} demonstrates a remarkable increase in Ca^{2+} entry during single APs, while the slower rise indicates greater heterogeneity across myocytes transduced with CaM mutants. N, Cumulative histograms of Ca^{2+} entry for CaM_{D130G} (red, left) and CaM_{F142L} (red, right), with the fit for CaM_{WT} reproduced in gray.

for electrically driven arrhythmias at the tissue and organ levels [28]. Similar results were obtained for expression of CaM_{D130G} (Figs. 1E–F, $APD_{80} = 915.3 \pm 231.7$ ms, $P < 0.001$; $SD_{cell} = 78.5$ ms, $P \leq 0.01$) and CaM_{F142L} (Figs. 1G–H, $APD_{80} = 864.9 \pm 320.1$ ms, $P < 0.001$; $SD_{cell} = 179.1$ ms, $P < 0.01$). The exemplar for CaM_{D130G} illustrates the occurrence of alternans (Fig. 1E), and that for CaM_{F142L} exemplifies simple APD prolongation. All these behaviors (Figs. 1C, E, G) could be observed in the presence of any of the CaM mutants and persist at faster pacing rates (Supplementary Fig. 2). Detailed parameters for action potential recordings are in Table 1 and Supplementary Table 1.

Table 1
Average values for APs recorded at 0.5 Hz pacing.

CaM	APD_{80} (ms)	$(dV/dt)_{max}$ (mV/ms)	V_{rest} (mV)[a]	V_{max} (mV)
WT	417.0 ± 6	119.9 ± 3.2	−62.0 ± 0.2	55.7 ± 0.4
D130G	824.2 ± 16*	112.5 ± 2.1	−61.3 ± 0.2	48.4 ± 0.6
D96V	973.6 ± 12*	139.5 ± 1.7	−62.6 ± 0.1	56.3 ± 0.3
F142L	874.8 ± 22*	131.7 ± 3.8	−61.8 ± 0.2	51.8 ± 0.5
N54I	391 ± 4.5	128.7 ± 1.4	−64.9 ± 0.3	53.6 ± 0.3
N98S	751.8 ± 5.8*	160.6 ± 1.0	−62.4 ± 0.1	58.1 ± 0.1

* $P < 0.01$.
[a] Values consistent with those expected for aGPVMs after one day in culture [56,57].

Beyond electrical disturbances, Ca^{2+} cycling dysfunction may also drive arrhythmogenesis [29]. Accordingly, we examined the effect of LQTS CaM mutant expression on intracellular Ca^{2+} transients. Fig. 1I displays the typical Ca^{2+} waveform in a myocyte expressing only CaM_{WT}. Ratiometric Indo-1 imaging was used to gauge Ca^{2+} activity, and data are shown as the mean ± SD drawn from multiple cells. The black trace plots the mean, and standard deviation bounds are shown by gray shadows. Upon expression of CaM_{D96V}, Ca^{2+} transients are markedly amplified and prolonged (Fig. 1J, red). Reproduction of the control CaM_{WT} waveform (gray) serves to emphasize the strong changes in Ca^{2+} activity. Likewise, expression of CaM_{D130G} and CaM_{F142L} produced similarly striking increases of Ca^{2+} transients (Figs. 1K–L). Representing these data in cumulative histogram format serves to emphasize the increased dispersion of peak Ca^{2+} transient amplitude produced by CaM mutants (Figs. 1M–N). Shown here are the cumulative probabilities of the area under Ca^{2+} transients (P_Q) for CaM_{WT} and CaM mutants as labeled. The precipitous rise of the wild-type distribution confirms the similarity of Ca^{2+} amplitudes among cells (Fig. 1M, black relation). By contrast, the sluggish rise of distributions for CaM mutants (Figs. 1M and N, red relations) reveals marked heterogeneity of Ca^{2+} transients among cells, as confirmed by significantly larger intra-cell standard deviations (gray bars, $P < 0.05$). Additionally, both diastolic Ca^{2+} concentrations and SR Ca^{2+} content were significantly elevated by overexpressing LQTS CaM mutants (Supplementary Fig. 3). In all, CaM mutants furnish the cellular substrates for Ca^{2+}-driven arrhythmias [29], by increasing amplitude and dispersion of Ca^{2+} transients, heightening diastolic Ca^{2+} concentration, and augmenting SR Ca^{2+} content.

3.2. LQTS calmodulin mutants suppress Ca^{2+}/CaM-mediated inactivation of $Ca_V1.2$ Ca^{2+} channels

The ability of naturally occurring LQTS CaM mutants to prolong and disperse action potentials was reminiscent of effects we and others observed previously under expression of man-made CaM mutants in the same and similar model systems [13,30]. There, many of the action potential effects could be attributed to the suppression of a Ca^{2+}/CaM-mediated inactivation (CDI) of $Ca_V1.2$ Ca^{2+} channels. We therefore tested for the effects of the naturally occurring LQTS-related CaM mutants on $Ca_V1.2$ CDI, heterologously expressed in HEK293 cells for maximal biophysical resolution. In this regard, $Ca_V1.2$ expression here included the use of an auxiliary β_{2a} subunit to better visualize CDI effects by minimizing voltage-dependent inactivation [21].

Fig. 2A displays exemplar currents of $Ca_V1.2$ channels coexpressed with CaM_{WT}. The sharp decay of Ca^{2+} current (red) evoked by a 30-mV depolarizing step is the well-known result of the CDI process. As confirmation, Ba^{2+} current (black) evoked in the same cell hardly decays, as Ba^{2+} binds poorly to CaM. Population data shown below (Figs. 2B–C) rounds out characterization of the baseline behavior of channels in the presence of CaM_{WT}. Fig. 2B displays the average of the peak normalized Ba^{2+} current as a function of step potentials, and Fig. 2C plots the fraction of peak current remaining after 300-ms depolarization to various voltages (r_{300}). The U-shaped Ca^{2+} r_{300} relation (red) recapitulates the classic hallmark of CDI [31,32], while the flat $Ba^{2+}r_{300}$ relation (black) confirms the lack of appreciable inactivation without activation of CaM. Hence, the difference between Ba^{2+} and Ca^{2+} r_{300} relations at 30 mV, as normalized by the corresponding Ba^{2+} r_{300} value, formally gauges the extent of CDI ($f_{300} = 0.690 \pm 0.028$).

Upon coexpressing $Ca_V1.2$ channels with mutant CaM_{D96V}, a starkly different functional profile is observed (Figs. 2D–F). Here, CDI is strongly suppressed ($f_{300} = -0.009 \pm 0.008$, $P < 0.001$), without shift in the voltage activation profile (Fig. 2E). Similarly, coexpression of channels with CaM_{D130G} or CaM_{F142L} also sharply diminished CDI (Figs. 2G–I and Figs. 2J–L, $f_{300} = -0.002 \pm 0.011$, $P < 0.001$ and 0.065 ± 0.005, $P < 0.001$, respectively). The above results were obtained with strong intracellular Ca^{2+} buffering by 10 mM BAPTA, to restrict Ca^{2+} elevations to those in the nanodomains of individual channels, and thereby minimize cell-to-cell variations owing to differences in current amplitudes. Importantly, however, under more physiological Ca^{2+} buffering (1 mM EGTA) that allows global elevation of Ca^{2+}, strong but incomplete blunting of CDI was produced by the CaM mutants (Supplementary Fig. 4). This residual CDI can be attributed to signaling

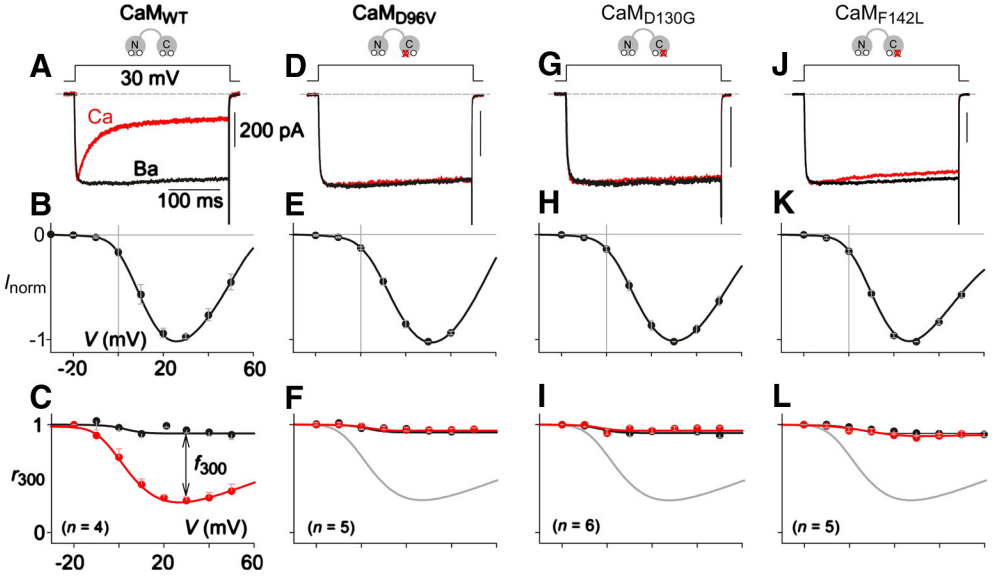

Fig. 2. LQTS CaM mutants diminish CDI in HEK293 cells. A, Exemplar currents evoked by 30-mV voltage step (top) in cells co-transfected with $Ca_V1.2$ and CaM_{WT}. CDI manifests as the stronger decay in Ca^{2+} (red) current as compared to Ba^{2+} (black). Ba^{2+} trace is scaled downward to match the peak of the Ca^{2+} trace, thus facilitating comparison of decay kinetics, and the scale bar for current references the Ca^{2+} trace, here and throughout. B, Average normalized peak current versus voltage relation obtained with Ba^{2+} for the same cells as in A. Data are plotted as mean ± SEM here and throughout. C, Population data for CDI across voltages. r_{300} measures the current remaining after 300 ms, after normalization to peak current. f_{300} is the difference between Ca^{2+} and Ba^{2+} at 30 mV, after normalization by the Ba^{2+} r_{300} value. D, Expression of CaM_{D96V} severely blunts CDI of $Ca_V1.2$. E, The current–voltage relation for the CaM_{D96V} scenario remains unaltered. F, Population data bears out the CaM_{D96V} reduction of CDI across voltages. For reference, the Ca^{2+} r_{300} curve for CaM_{WT} is reproduced in gray. G–L, CaM_{D130G} and CaM_{F142L} also induce dramatic CDI deficits. Format as in D–F.

through the N-terminal lobe of CaM (largely unaffected in LQTS CaM mutants), which is sensitive to sustained global elevation of calcium [33,34]. Overall, the naturally occurring CaM mutants suppressed $Ca_V1.2$ channel CDI, in a manner indistinguishable from that of a man-made mutant CaM_{34} molecules that selectively eliminate Ca^{2+} binding to the C- but not N-terminal lobe of this molecule [20,33,34].

By contrast, overexpressing CPVT CaM mutants had weaker effects on $Ca_V1.2$ channel CDI. CaM_{N54I} yielded no appreciable change in CDI compared to CaM_{WT} (Figs. 3A–C, $f_{300} = 0.583 \pm 0.043$, $P > 0.01$). On the other hand, CaM_{N98S} managed only to partially diminish CDI (Figs. 3F–H, $f_{300} = 0.367 \pm 0.023$, $P < 0.001$). Both results in Fig. 3 were obtained under high Ca^{2+} buffering conditions (10 mM BAPTA). Under more physiological Ca^{2+} buffering (1 mM EGTA), we observed a similar trend wherein CaM_{N54I} and CaM_{N98S} exerted at most modest diminution of CDI (Supplementary Fig. 5). To assess further the more integrative consequences of these CDI profiles (Figs. 3A–C, F–H), we investigated the effects of these CPVT CaM mutants within aGPVMs. As might be expected, action potentials in the presence of CaM_{N54I} were nearly identical to those with CaM_{WT} (Figs. 3D–E). On the other hand, CaM_{N98S} significantly prolonged action potentials (Figs. 3I–J, red $P < 0.01$) as compared to CaM_{WT} (gray). Additionally, intra-cell standard deviation (Fig. 3J, gray bar) was also larger than CaM_{WT} ($P < 0.05$), positioning CaM_{N98S} for moderate LQTS and affiliated arrhythmias. For CaM_{N54I}, the nearly complete lack of effect on CDI helps explain why this mutation was not associated with LQTS. Interestingly, the intermediate effects of CaM_{N98S} on CDI and action potentials match well with reports of LQTS in an unrelated patient [35].

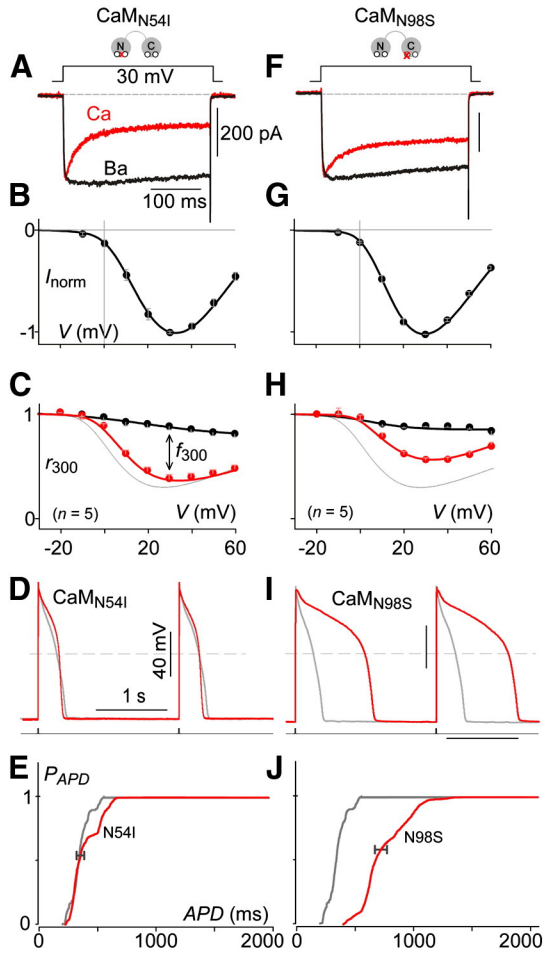

Fig. 3. CPVT CaM mutants exert weaker effects on CDI. A, Exemplar currents evoked by 30-mV voltage step (top) in HEK293 cells co-transfected with $Ca_V1.2$ and CaM_{N54I}. Here, coexpression of CaM_{N54I} did not disrupt CDI compared to CaM_{WT} (Fig. 2A). B, Average normalized peak current–voltage relationship for same cells as in A. Compared to CaM_{WT} (Fig. 2B), there is no shift in voltage activation. C, Voltage dependence of r_{300} values for Ca^{2+} (red) and Ba^{2+} (black). Ca^{2+} relation for CaM_{WT} configuration reproduced in gray for reference. No significant alteration of CDI across all test voltages. D–E, Coexpression of CaM_{N54I} does not appreciably effect action potentials (red) as compared to co-expression of CaM_{WT} (gray). Format as in Fig. 1. Data for panel E from 679 action potentials drawn from 6 myocytes. F, Expression of CaM_{N98S}, however, modestly diminishes CDI, without affecting voltage activation (G). H, Population data of r_{300} values confirm a small, but significant reduction of CDI across voltages. I–J, Overexpression of CaM_{N98S} has the ability to lengthen and increase heterogeneity of action potentials ($P < 0.01$). Format as in Fig. 1B. Horizontal error bars in panels E and J display standard deviation of APD_{80} within cells. Data for panel J from 1100 action potentials drawn from 6 myocytes.

Thus far, we have demonstrated the ability of the naturally occurring LQTS CaM mutants to markedly attenuate CDI of $Ca_V1.2$ channels heterologously expressed in HEK293 cells, to facilitate biophysical resolution. Nonetheless, we next wondered whether similar effects would be observed in native L-type Ca^{2+} currents, as present in the same aGPVMs as used in Fig. 1. Fig. 4A displays exemplar L-type currents evoked under whole-cell voltage clamp, using 10 mM BAPTA as the intracellular Ca^{2+} buffer, so as to mimic the condition of Fig. 2. Ryanodine (5 μM) was included in the intracellular dialyzate to eliminate phasic Ca^{2+} release from the sarcoplasmic reticulum, and limit CDI to that driven by Ca^{2+} entry through individual L-type Ca^{2+} channels [36]. We again observed strong CDI when Ca^{2+} was used as the charge carrier (red) as compared to a limited amount of voltage-dependent inactivation (VDI) seen in the Ba^{2+} current (black). This additional VDI component is expected in this native setting due to a mix of endogenous beta subunits [37,38], compared to the pure population of β_{2a} subunits utilized in HEK293 cell experiments. That said, the baseline f_{300} value estimating isolated CDI in control myocytes (Figs. 4A–C) was nonetheless 0.67 ± 0.04 (obtained at 20-mV step), which is quite similar to that obtained in recombinant channel expression experiments (Fig. 2C). Likewise, population data shows a similar current–voltage relationship and U-shaped Ca^{2+} r_{300} curve (Figs. 4B–C). Importantly, expression of mutant CaM_{D96V} essentially abolished CDI in this native setting ($f_{300} = -0.18 \pm 0.03$, $P < 0.001$, Figs. 4D–F) and so did CaM_{D130G} and CaM_{F142L} ($f_{300} = 0.02 \pm 0.09$, $P < 0.001$, Figs. 4G–I and -0.09 ± 0.03, $P < 0.001$, Figs. 4J–L, respectively), supporting a strong mechanistic link between $Ca_V1.2$ channel deficits and the LQTS effects seen in patients carrying the CaM mutations.

3.3. Limited expression of LQTS CaM molecules still affects $Ca_V1.2$ channel CDI

We have so far demonstrated that strong overexpression of LQTS-associated CaM molecules in myocytes can produce both strongly dysfunctional electrical and Ca^{2+} cycling, and potently diminished CDI. However, in the actual related patient population, only one of six alleles encodes a mutant CaM, while the other alleles would elaborate wild-type CaM. Accordingly, we would anticipate that only a limited fraction of CaM molecules would bear the pathogenic mutation [10]. How then could the significant cardiac deficits encountered by patients be rationalized? Previous mechanistic studies of L-type channel CDI offer a potential explanation. In particular, it has been shown that for CDI to occur, channels must initially preassociate with a Ca^{2+}-free CaM (apoCaM), to which subsequent Ca^{2+} binding triggers CDI [15,39]. That is, bulk CaM in the cytoplasm does not appreciably trigger CDI. Thus, if LQTS-associated mutant CaM molecules can still preassociate on par with wild-type CaM, then a sizeable fraction of channels would be bound to mutant CaM, and thus unable to undergo strong CDI (Figs. 2–3). Thus, the overall decrease in CDI should be appreciable, reflecting the aggregate fractional presence of mutant CaM in cells.

Accordingly, we utilized a well-established live-cell FRET two-hybrid binding assay to determine whether mutant CaMs can still interact with $Ca_V1.2$, in a manner similar to wild-type CaM. Fig. 5A (top) cartoons the relevant sites of apoCaM interaction with $Ca_V1.2$ channels, in particular the CI region of the channel carboxy tail. Our FRET assay therefore paired the $Ca_V1.2$ CI region with CaM (Fig. 5A, bottom). As baseline reference, Fig. 5B shows the canonical binding curve between

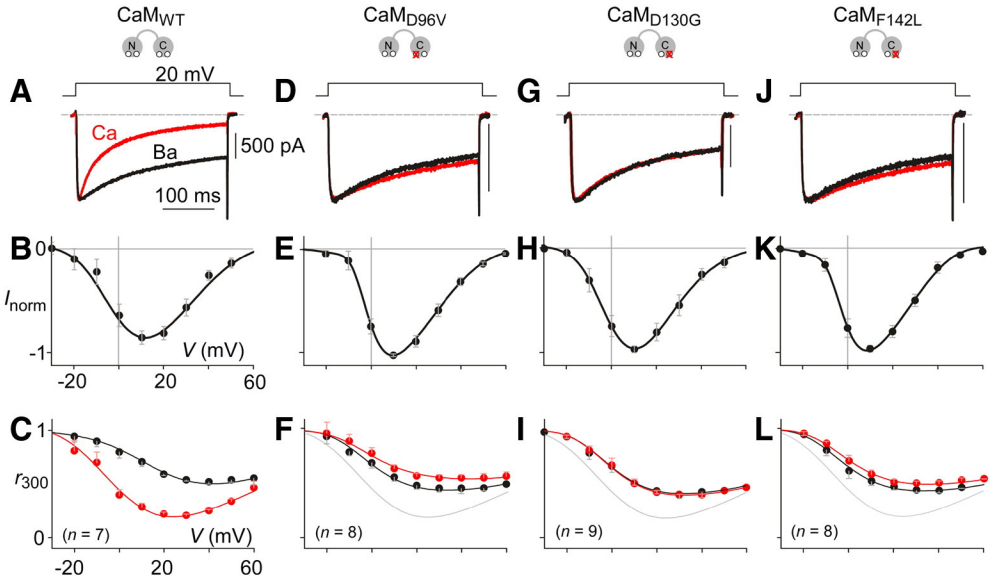

Fig. 4. CaM mutants diminish CDI in aGPVMs. A, CDI in native LTCCs recorded from one-day-old aGPVMs transduced with CaM_{WT}. Exemplar current traces elicited by a 20-mV voltage step (top) display strong CDI with Ca^{2+} (red), and a small amount VDI with Ba^{2+} (black). B, Average normalized peak current–voltage relation obtained in Ba^{2+} for the same cells as in A. C, Population data for CDI across voltages. f_{300} is measured at 20 mV. D, Expression of CaM_{D96V} severely blunts CDI in the native setting. E, Current–voltage relation in the presence of CaM_{D96V} remains unaltered. F, Population data confirms the CaM_{D96V} reduction of CDI across voltages. For reference, the Ca^{2+} r_{300} curve for CaM_{WT} is reproduced in gray. G–L, CaM_{D130G} and CaM_{F142L} also induce dramatic CDI deficits. Format as in D–F.

the CI region and CaM_{WT}, where this plot displays the acceptor-centric FRET efficiency of interaction (E_A) as a function of the relative free concentration of donor-tagged molecules D_{free} (cerulean-CaM_{WT}). The curve resembles a typical binding reaction, and the D_{free} that produces half-maximal E_A yields an effective dissociation constant ($K_{d,EFF}$) of 12,000 D_{free} units [5]. Reassuringly, all three mutant CaM molecules bind at least as well as wild-type CaM (Figs. 5B–E), demonstrating that mixed expression of mutant and wild-type CaM will result in some fraction of channels bound to mutant CaM.

To test this notion quantitatively, we first devised simple means to control the expression ratio of wild-type to mutant CaM molecules ($\hat{\gamma}$) (Supplementary Note 1.6). Then, we performed whole-cell electrophysiology experiments to test explicitly whether the strength of CDI in $Ca_V1.2$ channels would be graded by different $\hat{\gamma}$ values, just as anticipated by the relative binding affinities of channels for mutant versus wild-type apoCaM (Figs. 5B–E). Here, our approach was to strongly overexpress variable ratios of such molecules so that the contribution of endogenous CaM would be negligible. If such a scenario were to hold true, we could quantitatively predict the aggregate CDI strength (*CDI*) as a function of the protein expression ratio of wild-type to mutant CaM, as the Langmuir equation in Fig. 6A (Supplementary Note 1.7). CDI_{WT} is the full-strength CDI measured with only wild-type CaM strongly overexpressed, and $K_{d/WT}$ and $K_{d/MUT}$ are the dissociation constants for channel preassociation with wild-type and mutant apoCaM, as specified in Figs. 5B–E. Fig. 6B plots this relation explicitly as the smooth black curve. Colored data symbols, with corresponding exemplar traces in Fig. 6C, nicely decorate this Langmuir function, as do data from numerous other cells (open symbols in Fig. 6B). Similar results were obtained for the other two LQTS-associated CaM mutants (Supplementary Fig. 9). Thus, mixtures of wild-type and mutant CaM would weaken L-type channel CDI as predicted by the relative channel affinities for these two molecules in their Ca^{2+}-free form. Based on the relative expression profile of each *CALM* during infancy [10], heterozygous D96V mutation on *CALM2* gene yields $\hat{\gamma}$ ~7, predicting the substantial decrement of CDI indicated by the light rose shading in Fig. 6B, likely sufficient to appreciably prolong APDs [30,40]. Interestingly, the corresponding prediction for a

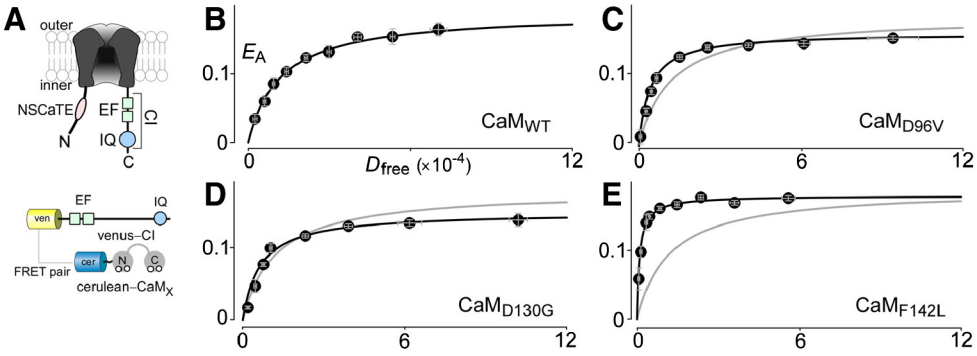

Fig. 5. Mutant CaMs bind to $Ca_V1.2$ channels at least as well as wild-type CaM. A, Cartoon depicting CaM interaction domains on the $Ca_V1.2$ calcium channel (CI segment). Below, construct schematics depicting FRET interaction pairs used for binding assessment. B, The canonical FRET binding curve between the CI region and CaM_{WT}. In particular, an acceptor-centric FRET efficiency (E_A) is plotted as a function of the relative free concentration of donor-tagged molecules D_{free} (cerulean-CaM_{WT}). $K_{d/EFF}$ for CaM_{WT} binding to CI region is 12,000 D_{free} units [5]. C–E, FRET binding curves between the CI region and CaM_{D96V} (C), CaM_{D130G} (D) and CaM_{F142L} (E). $K_{d/EFF}$ are 4000, 6500, and 1000 D_{free} units, respectively. The binding curve for CaM_{WT} is reproduced in gray for reference.

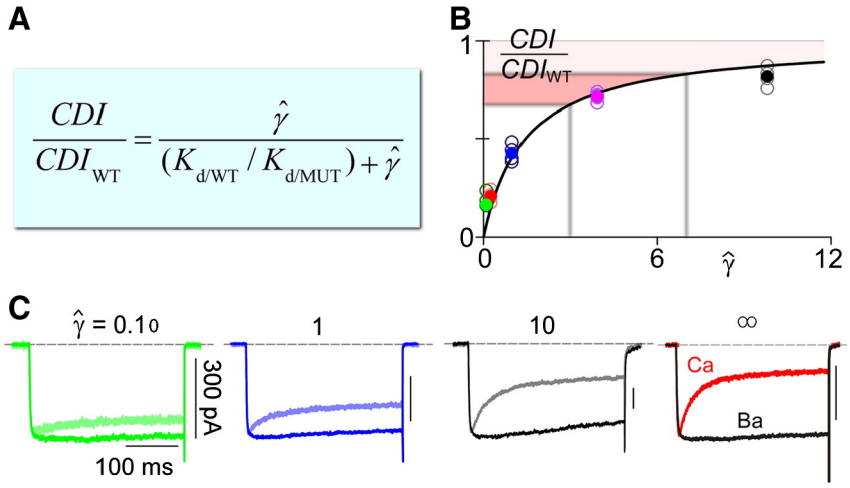

Fig. 6. Dose-dependent effect of mutant CaMs. A, Langmuir equation relating the extent of CDI and wild-type versus mutant CaM expression ratio $\hat{\gamma}$. B, Predicted CDI as a function of $\hat{\gamma}$ (black). Solid circles indicate average data for each ratio $\hat{\gamma}$; open circles pertain to data for individual cells. Light rose shaded region indicates the deficit in CDI expected for a expression ratio corresponding to heterozygous mutation in *CALM2* gene, while dark rose shaded region indicates predicted extent of CDI reduction for homozygous mutation. C, Exemplar current traces with the colors corresponding to the Langmuir plot in B. For each set of records, the Ca^{2+} trace is the lighter color waveform, and the corresponding Ba^{2+} trace is normalized to the peak of the Ca^{2+} trace for comparison of decay kinetics. Scale bar corresponds to Ca^{2+}. Exemplar traces on far right are from a cell expressing CaM_{WT} only ($\hat{\gamma} = \infty$), as reproduced from Fig. 2A for reference.

hypothetical homozygous scenario ($\hat{\gamma} \sim 3$, dark rose shading) suggests a severe reduction in CDI, potentially incompatible with life. This would perhaps predict the absence of living homozygous individuals.

In all, we would argue that the electrical and calcium dysfunction affiliated with LQTS-associated CaM mutations arises as summarized in Fig. 7. Mutant CaM elaborated by a single allele among three *CALM* genes would yield a mixture of wild-type and mutant CaM molecules, as specified by the expression ratio $\hat{\gamma}$. Because channels must first preassociate with apoCaM to undergo subsequent CDI, this fractional expression of mutant CaM would produce graded reduction of overall CDI in myocytes, as demonstrated in Fig. 6. This decrement of Ca^{2+} feedback inhibition would elaborate abnormally long action potentials and QT intervals [13], likely in a cell-specific manner dependent on both the precise value of $\hat{\gamma}$, and complex interactions with the configuration of other ion-channel and Ca^{2+}-cycling molecules present. The latter interaction factors likely contribute to the impressive dispersion of properties documented in Fig. 1. Given the variable propensity for action potential prolongation and calcium augmentation within different cells, arrhythmogenic behavior at the tissue and organ levels could thus result. Although other effects of mutant CaM molecules are likely to contribute to overall pathogenesis (Fig. 7, gray pathway with arrow), this study furnishes strong evidence that a major underlying mechanism concerns the attenuation of L-type calcium channel CDI by the presence of LQTS-associated mutant CaM molecules. This outcome furnishes at least one major molecular target that merits scrutiny for potential therapeutics.

4. Discussion

Our experiments demonstrate that CaM bearing LQTS mutations induce the cellular substrates that would favor a LQTS phenotype. Acute introduction of LQTS mutant CaMs into aGPVMs leads to: (1) electrical disturbances including prolonged APD and electrical alternans, as well as (2) Ca^{2+} cycling disturbances, such as increased Ca^{2+} transients and SR Ca^{2+} load. Importantly, such alterations manifested in a highly dispersed fashion across and within cells, thus furnishing a critical ingredient for arrhythmogenesis at the tissue and organ levels [28]. The present study also clearly indicates that a key contributor to these effects involves the disruption of L-type channel CDI by LQTS CaM mutants. Such CDI attenuation would elaborate increased Ca^{2+} current during phases 2 and 3 of the action potentials, thus prolonging APD and increasing SR Ca^{2+} load. Finally, we have established one scenario by which a small fraction of CaM mutants would suffice to create an appreciable prolongation of action potentials. Preassociation of apoCaM to the $Ca_V1.2$ channels plays a critical role, enabling a fraction of channels to be occupied by the CaM mutants with resulting failure to undergo CDI.

Interestingly, CaM mutants commonly affiliated with CPVT exhibited negligible or weaker effects on action potential duration and L-type channel CDI. The complete lack of effect of CaM_{N54I} on CDI and action potential duration is well explained by its near wild-type Ca^{2+} binding affinity [41], and these molecular and cellular outcomes fit nicely with

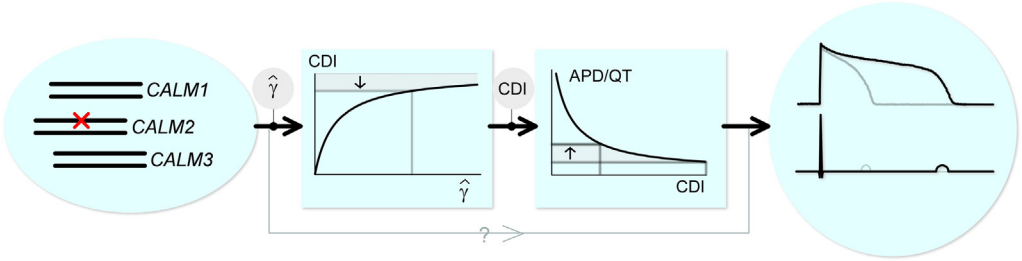

Fig. 7. Proposed mechanism of electrical and calcium dysfunction for LQTS CaM mutants. Flow diagram schematizing how heterozygous *CALM2* mutation might lead to fractional decrease in CDI, yielding action potential prolongation and ultimately long QT phenomena.

the lack of appreciable QT prolongation in corresponding probands [9]. This CPVT-associated mutant could nonetheless interact with other targets like RyR2 calcium release channels to potentially contribute to pathogenesis [41]. On the other hand, the CPVT CaM mutant N98S is capable of producing either CPVT [9,41] or LQTS in patients [35]. This dual effect may well arise from the overlapping effects of these mutations on multiple CaM targets in the heart. Indeed, CaM_{N98S} turned out to both reduce L-type channel CDI and moderately prolong cardiac action potentials (Fig. 3). The intermediate effects of this CaM mutant thus rationalize how LQTS or CPVT may become the more prominent clinical phenotype, perhaps as a function of differing expression levels among patients.

In addition to L-type ($Ca_V1.2$) channels, other molecular targets of CaM remain as potential contributors to LQTS pathogenesis. Focusing in particular on targets that preassociate with Ca^{2+}-free CaM, voltage-gated Na channels [42] ($Na_V1.5$) and slow delayed rectifier K channels [43] (I_{Ks}) loom among likely targets. In $Na_V1.5$ channels, Ca^{2+}/CaM is proposed to both facilitate initial opening and stabilize the inactivated state [42]. However, a recent study reports that LQTS CaM mutants lacked significant effects on most splice variants of $Na_V1.5$ channels, though the CaM_{D130G} mutant appeared to moderately enhance persistent current in one fetal splice variant [44]. For I_{Ks}, Ca^{2+}-free CaM may help traffic channels to plasmalemma [45], and Ca^{2+}/CaM is believed to facilitate opening. In fact, mutations in I_{Ks} that disrupt CaM binding result in decreased K current, thus causing LQTS [43,46]. More broadly, because CaM regulates many other Ca^{2+} channel subtypes, including those predominate in neurons and immune cells, disruption of CDI could lead to a multi-system disorder similar to Timothy syndrome [47–49]. It may well be that extra-cardiac effects are also present in patients possessing LQTS CaM mutants, but that these effects were not recognized in the face of immediately life-threatening cardiac-related sequelae. For other CaM-modulated signaling molecules that do not preassociate with Ca^{2+}-free CaM, the present study would suggest that a limited fraction of LQTS CaM mutants would matter little. Only when the fraction of CaM mutants approaches unity would this class of targets be predicted to exhibit altered function. Key members of this class of CaM targets in cardiac myocytes would include Ca^{2+}/CaM-dependent kinase II (CaMKII) and calcineurin (CN). CaMKII has been argued to influence the electrical properties of cardiomyocytes by phosphorylation of ryanodine receptors, phospholamban, SERCA, and L-type Ca^{2+} channels, all of which could alter electrical and Ca^{2+} function [50]. By contrast, the Ca^{2+}/CaM-activated phosphatase CN dephosphorylates numerous targets including the transcription factor NFAT, implicated in regulating expression levels of numerous ion channels in heart [51]. Nonetheless, if our insights are correct regarding the necessary role of target preassociation with apoCaM to amplify the effects of a limited fraction of CaM mutants, molecules like CaMKII and CN may play little role in the LQTS phenotype at hand.

Even before testing for a role of the additional target molecules alluded to above, potential targeted therapeutic strategies in patients expressing LQTS CaM mutants are suggested by our finding that LTCC dysfunction likely contributes in this particular setting. In addition to beta-adrenergic blockade, as per the general standard of care for LQTS patients, immediate benefits may arise by seeking appropriate modulators of LTCCs such as roscovitine, which has demonstrated beneficial effects within certain in vitro models of LTCC-related LQTS [52]. Additionally, a recent study implicates a non-linear threshold effect between the extent of CDI diminution in LTCCs and onset of outright arrhythmias [53], rather than a continuously graded interrelation. Accordingly, only a few-fold decrease in the fraction of CaM mutants ($\hat{\gamma}$) may yield marked improvement of electrical stability and decrease in the incidence of cardiac arrest. The limited alteration of $\hat{\gamma}$ potentially required to bring about these benefits may considerably improve the feasibility of devising novel therapies towards this end.

Although the prevalence of diseases caused by *de novo* CaM mutations is limited, investigating their pathogenesis may offer revealing opportunities to expand our basic knowledge of LQTS-related arrhythmogenesis. Moreover, additional discoveries of CaM mutations will help expand our database of related genotype-phenotype correlations, lending further resources for understanding. Indeed, following the first discoveries of CaM mutations, three more recent preliminary studies [35,54,55] have uncovered further CaM-affiliated arrhythmias. These include the following, listed according to gene and syndrome: D134H (*CALM2*; LQTS), N98S (*CALM2*; LQTS), D132F (*CALM2*; LQTS and CPVT), N54I (*CALM1*; LQTS and/or sudden unexplained death in the young (SUDY)), A103V (*CALM3*; CPVT and/or SUDY), F90L (*CALM1*; ventricular fibrillation). These exciting discoveries suggest that a small yet substantial population of patients with CaM mutations is emerging, thus necessitating the inclusion of *CALM* genes in genetic test panels for LQTS and CPVT, and providing added motivation for the discovery of new therapies. In this light, it may be warranted to dub this expanding group of CaM-related disorders as calmodulinopathies.

Sources of funding

This research was supported by the Predoctoral Fellowship from the American Heart Association (W.B.L.); R37HL076795 MERIT (D.T.Y.); and R01HL083374 (A.L.G.).

Disclosures

None.

Acknowledgments

We would like to thank Philemon Yang and Wanjun Yang with their help in adenovirus amplification, and Manu Ben Johny for advice on optimizing FRET two-hybrid assays of apoCaM with the CI region of $Ca_V1.2$ channels, and initial electrophysiological characterization of CPVT CaM mutants.

Appendix A. Supplementary data

Supplementary data to this article can be found online at http://dx.doi.org/10.1016/j.yjmcc.2014.04.022.

References

[1] Pitt GS. Calmodulin and CaMKII as molecular switches for cardiac ion channels. Cardiovasc Res 2007;73:641–7.
[2] Hoeflich KP, Ikura M. Calmodulin in action: diversity in target recognition and activation mechanisms. Cell 2002;108:739–42.
[3] Ikeda S, He A, Kong SW, Lu J, Bejar R, Bodyak N, et al. MicroRNA-1 negatively regulates expression of the hypertrophy-associated calmodulin and Mef2a genes. Mol Cell Biol 2009;29:2193–204.
[4] Chambers JS, Thomas D, Saland L, Neve RL, Perrone-Bizzozero NI. Growth-associated protein 43 (GAP-43) and synaptophysin alterations in the dentate gyrus of patients with schizophrenia. Prog Neuropsychopharmacol Biol Psychiatry 2005;29:283–90.
[5] Bazzazi H, Ben Johny M, Adams PJ, Soong TW, Yue DT. Continuously tunable Ca(2+) regulation of RNA-edited CaV1.3 channels. Cell Rep 2013;5:367–77.
[6] Lee D, Lee SY, Lee EN, Chang CS, Paik SR. alpha-Synuclein exhibits competitive interaction between calmodulin and synthetic membranes. J Neurochem 2002;82:1007–17.
[7] Chan CS, Guzman JN, Ilijic E, Mercer JN, Rick C, Tkatch T, et al. 'Rejuvenation' protects neurons in mouse models of Parkinson's disease. Nature 2007;447:1081–6.
[8] Wang B, Sullivan KM, Beckingham K. Drosophila calmodulin mutants with specific defects in the musculature or in the nervous system. Genetics 2003;165:1255–68.
[9] Nyegaard M, Overgaard MT, Sondergaard MT, Vranas M, Behr ER, Hildebrandt LL, et al. Mutations in calmodulin cause ventricular tachycardia and sudden cardiac death. Am J Hum Genet 2012;91:703–12.
[10] Crotti L, Johnson CN, Graf E, De Ferrari GM, Cuneo BF, Ovadia M, et al. Calmodulin mutations associated with recurrent cardiac arrest in infants. Circulation 2013;127:1009–17.
[11] Mori MX, Erickson MG, Yue DT. Functional stoichiometry and local enrichment of calmodulin interacting with Ca^{2+} channels. Science 2004;304:432–5.
[12] Saucerman JJ, Bers DM. Calmodulin binding proteins provide domains of local Ca^{2+} signaling in cardiac myocytes. J Mol Cell Cardiol 2012;52:312–6.

[13] Alseikhan BA, DeMaria CD, Colecraft HM, Yue DT. Engineered calmodulins reveal the unexpected eminence of Ca^{2+} channel inactivation in controlling heart excitation. Proc Natl Acad Sci U S A 2002;99:17185–90.
[14] Ben Johny M, Yang PS, Bazzazi H, Yue DT. Dynamic switching of calmodulin interactions underlies Ca^{2+} regulation of CaV1.3 channels. Nat Commun 2013;4:1717.
[15] Erickson MG, Alseikhan BA, Peterson BZ, Yue DT. Preassociation of calmodulin with voltage-gated Ca(2+) channels revealed by FRET in single living cells. Neuron 2001;31:973–85.
[16] Liu X, Yang PS, Yang W, Yue DT. Enzyme-inhibitor-like tuning of Ca(2+) channel connectivity with calmodulin. Nature 2010;463:968–72.
[17] Pitt GS, Zuhlke RD, Hudmon A, Schulman H, Reuter H, Tsien RW. Molecular basis of calmodulin tethering and Ca^{2+}-dependent inactivation of L-type Ca^{2+} channels. J Biol Chem 2001;276:30794–802.
[18] Joshi-Mukherjee R, Dick IE, Liu T, O'Rourke B, Yue DT, Tung L. Structural and functional plasticity in long-term cultures of adult ventricular myocytes. J Mol Cell Cardiol 2013;65C:76–87.
[19] Tang ZZ, Liang MC, Lu S, Yu D, Yu CY, Yue DT, et al. Transcript scanning reveals novel and extensive splice variations in human l-type voltage-gated calcium channel, Cav1.2 alpha1 subunit. J Biol Chem 2004;279:44335–43.
[20] Peterson BZ, DeMaria CD, Adelman JP, Yue DT. Calmodulin is the Ca^{2+} sensor for Ca^{2+}-dependent inactivation of L-type calcium channels. Neuron 1999;22:549–58.
[21] Dafi O, Berrou L, Dodier Y, Raybaud A, Sauve R, Parent L. Negatively charged residues in the N-terminal of the AID helix confer slow voltage dependent inactivation gating to CaV1.2. Biophys J 2004;87:3181–92.
[22] Lambert RC, Maulet Y, Dupont JL, Mykita S, Craig P, Volsen S, et al. Polyethylenimine-mediated DNA transfection of peripheral and central neurons in primary culture: probing Ca^{2+} channel structure and function with antisense oligonucleotides. Mol Cell Neurosci 1996;7:239–46.
[23] Bers DM, Patton CW, Nuccitelli R. A practical guide to the preparation of Ca(2+) buffers. Methods Cell Biol 2010;99:1–26.
[24] Barry PH. JPCalc, a software package for calculating liquid junction potential corrections in patch-clamp, intracellular, epithelial and bilayer measurements and for correcting junction potential measurements. J Neurosci Methods 1994;51:107–16.
[25] Sathaye A, Bursac N, Sheehy S, Tung L. Electrical pacing counteracts intrinsic shortening of action potential duration of neonatal rat ventricular cells in culture. J Mol Cell Cardiol 2006;41:633–41.
[26] Bassani JW, Bassani RA, Bers DM. Calibration of indo-1 and resting intracellular [Ca]i in intact rabbit cardiac myocytes. Biophys J 1995;68:1453–60.
[27] McKemy DD, Welch W, Airey JA, Sutko JL. Concentrations of caffeine greater than 20 mM increase the indo-1 fluorescence ratio in a Ca(2+)-independent manner. Cell Calcium 2000;27:117–24.
[28] Arevalo H, Rodriguez B, Trayanova N. Arrhythmogenesis in the heart: multiscale modeling of the effects of defibrillation shocks and the role of electrophysiological heterogeneity. Chaos 2007;17:015103.
[29] Xie LH, Weiss JN. Arrhythmogenic consequences of intracellular calcium waves. Am J Physiol Heart Circ Physiol 2009;297:H997-1002.
[30] Mahajan A, Sato D, Shiferaw Y, Baher A, Xie LH, Peralta R, et al. Modifying L-type calcium current kinetics: consequences for cardiac excitation and arrhythmia dynamics. Biophys J 2008;94:411–23.
[31] Brehm P, Eckert R. Calcium entry leads to inactivation of calcium channel in *Paramecium*. Science 1978;202:1203–6.
[32] Brehm P, Eckert R, Tillotson D. Calcium-mediated inactivation of calcium current in *Paramecium*. J Physiol 1980;306:193–203.
[33] Dick IE, Tadross MR, Liang H, Tay LH, Yang W, Yue DT. A modular switch for spatial Ca^{2+} selectivity in the calmodulin regulation of CaV channels. Nature 2008;451:830–4.
[34] Tadross MR, Dick IE, Yue DT. Mechanism of local and global Ca^{2+} sensing by calmodulin in complex with a Ca^{2+} channel. Cell 2008;133:1228–40.
[35] Makita N, Yagihara N, Crotti L, Johnson CN, Beckermann B-M, Shigemizu D, et al. Abstract 13371: CALM2 mutations associated with atypical juvenile long QT syndrome. Circulation 2013;128:A13371.
[36] Grandi E, Morotti S, Ginsburg KS, Severi S, Bers DM. Interplay of voltage and Ca-dependent inactivation of L-type Ca current. Prog Biophys Mol Biol 2010;103:44–50.
[37] Hullin R, Singer-Lahat D, Freichel M, Biel M, Dascal N, Hofmann F, et al. Calcium channel beta subunit heterogeneity: functional expression of cloned cDNA from heart, aorta and brain. EMBO J 1992;11:885–90.
[38] Olcese R, Qin N, Schneider T, Neely A, Wei X, Stefani E, et al. The amino terminus of a calcium channel beta subunit sets rates of channel inactivation independently of the subunit's effect on activation. Neuron 1994;13:1433–8.
[39] Zuhlke RD, Pitt GS, Deisseroth K, Tsien RW, Reuter H. Calmodulin supports both inactivation and facilitation of L-type calcium channels. Nature 1999;399:159–62.
[40] Morotti S, Grandi E, Summa A, Ginsburg KS, Bers DM. Theoretical study of L-type Ca(2+) current inactivation kinetics during action potential repolarization and early after depolarizations. J Physiol 2012;590:4465–81.
[41] Hwang HS, Nitu FR, Yang Y, Walweel K, Pereira L, Johnson CN, et al. Divergent regulation of ryanodine receptor 2 calcium release channels by arrhythmogenic human calmodulin missense mutants. Circ Res 2014;114:1114–24.
[42] Van Petegem F, Lobo PA, Ahern CA. Seeing the forest through the trees: towards a unified view on physiological calcium regulation of voltage-gated sodium channels. Biophys J 2012;103:2243–51.
[43] Shamgar L, Ma L, Schmitt N, Haitin Y, Peretz A, Wiener R, et al. Calmodulin is essential for cardiac IKS channel gating and assembly: impaired function in long-QT mutations. Circ Res 2006;98:1055–63.
[44] Murphy LL, Campbell CM, Crotti L, Johnson CN, Kunic JD, Schwartz PJ, et al. Abstract 14999: calmodulin mutation associated with neonatal long-QT syndrome evokes increased persistent sodium current from a fetal Nav1.5 splice variant. Circulation 2013;128:A14999.
[45] Roden DM. A new role for calmodulin in ion channel biology. Circ Res 2006;98:979–81.
[46] Ghosh S, Nunziato DA, Pitt GS. KCNQ1 assembly and function is blocked by long-QT syndrome mutations that disrupt interaction with calmodulin. Circ Res 2006;98:1048–54.
[47] Raybaud A, Dodier Y, Bissonnette P, Simoes M, Bichet DG, Sauve R, et al. The role of the GX9GX3G motif in the gating of high voltage-activated Ca^{2+} channels. J Biol Chem 2006;281:39424–36.
[48] Splawski I, Timothy KW, Decher N, Kumar P, Sachse FB, Beggs AH, et al. Severe arrhythmia disorder caused by cardiac L-type calcium channel mutations. Proc Natl Acad Sci U S A 2005;102:8089–96 discussion 6–8.
[49] Splawski I, Timothy KW, Sharpe LM, Decher N, Kumar P, Bloise R, et al. Ca(V)1.2 calcium channel dysfunction causes a multisystem disorder including arrhythmia and autism. Cell 2004;119:19–31.
[50] Rokita AG, Anderson ME. New therapeutic targets in cardiology: arrhythmias and Ca^{2+}/calmodulin-dependent kinase II (CaMKII). Circulation 2012;126:2125–39.
[51] Eder P, Molkentin JD. TRPC channels as effectors of cardiac hypertrophy. Circ Res 2011;108:265–72.
[52] Yazawa M, Hsueh B, Jia X, Pasca AM, Bernstein JA, Hallmayer J, et al. Using induced pluripotent stem cells to investigate cardiac phenotypes in Timothy syndrome. Nature 2011;471:230–4.
[53] Dick IE, Joshi-Mukherjee R, Yue DT. Nonlinear behavior in the induction of arrhythmias by channels bearing Timothy syndrome mutations. Biophysical Society. San Diego. Biophys J 2012:542a.
[54] Boczek NJ, Will ML, Loporcaro CG, Tester DJ, Ackerman MJ. Abstract 14699: spectrum and prevalence of CALM1, CALM2, and CALM3 mutations in long QT Syndrome, catecholaminergic polymorphic ventricular tachycardia, idiopathic ventricular fibrillation, and sudden unexplained death in the young. Circulation 2013;128:A14699.
[55] Marsman RF, Barc J, Beekman L, Alders M, Dooijes D, van den Wijngaard A, et al. A mutation in CALM1 encoding calmodulin in familial idiopathic ventricular fibrillation in childhood and adolescence. J Am Coll Cardiol 2014;63:259–66.
[56] Busch AE, Suessbrich H, Waldegger S, Sailer E, Greger R, Lang H, et al. Inhibition of IKs in guinea pig cardiac myocytes and guinea pig IsK channels by the chromanol 293B. Pflugers Arch 1996;432:1094–6.
[57] Mitcheson JS, Hancox JC, Levi AJ. Action potentials, ion channel currents and transverse tubule density in adult rabbit ventricular myocytes maintained for 6 days in cell culture. Pflugers Arch 1996;431:814–27.

Supplementary Information

Calmodulin Mutants Associated with Long QT Syndrome Prevent Inactivation of Cardiac L-type Ca^{2+} Currents and Promote Proarrhythmic Behavior in Ventricular Myocytes

Limpitikul *et al*, Journal of Molecular and Cellular Cardiology

Table of Contents

1. Additional Data and Detailed Derivation of CaM Ratio Equation

1.1 WT CaM overexpression has minimal effects on action potential morphology or duration.

To ensure that transduction of heterologous CaM via adenovirus does not alter the baseline action potential, we compared the action potentials of non-transduced aGPVMs with those of aGPVMs transduced with CaM_{WT}. Supplementary Figures 1A-B compare action potential waveforms from uninfected one-day-old aGPVMs (endogenous CaM) and with one-day old aGPVMs overexpressing CaM_{WT}. There was no observable change in the action potential shape or duration at either 0.5 or 1 Hz pacing. Population data shown in panel C not only demonstrate negligible change in action potential duration due to expression of CaM_{WT}, but document just how stable and reproducible the action potential durations of these cells are. These data thus confirm these one-day old aGPVMs as a robust model for the study of action potential perturbations. In all, transduction of CaM via adenovirus is well tolerated by aGPVMs, producing no appreciable perturbations across multiple pacing frequencies.

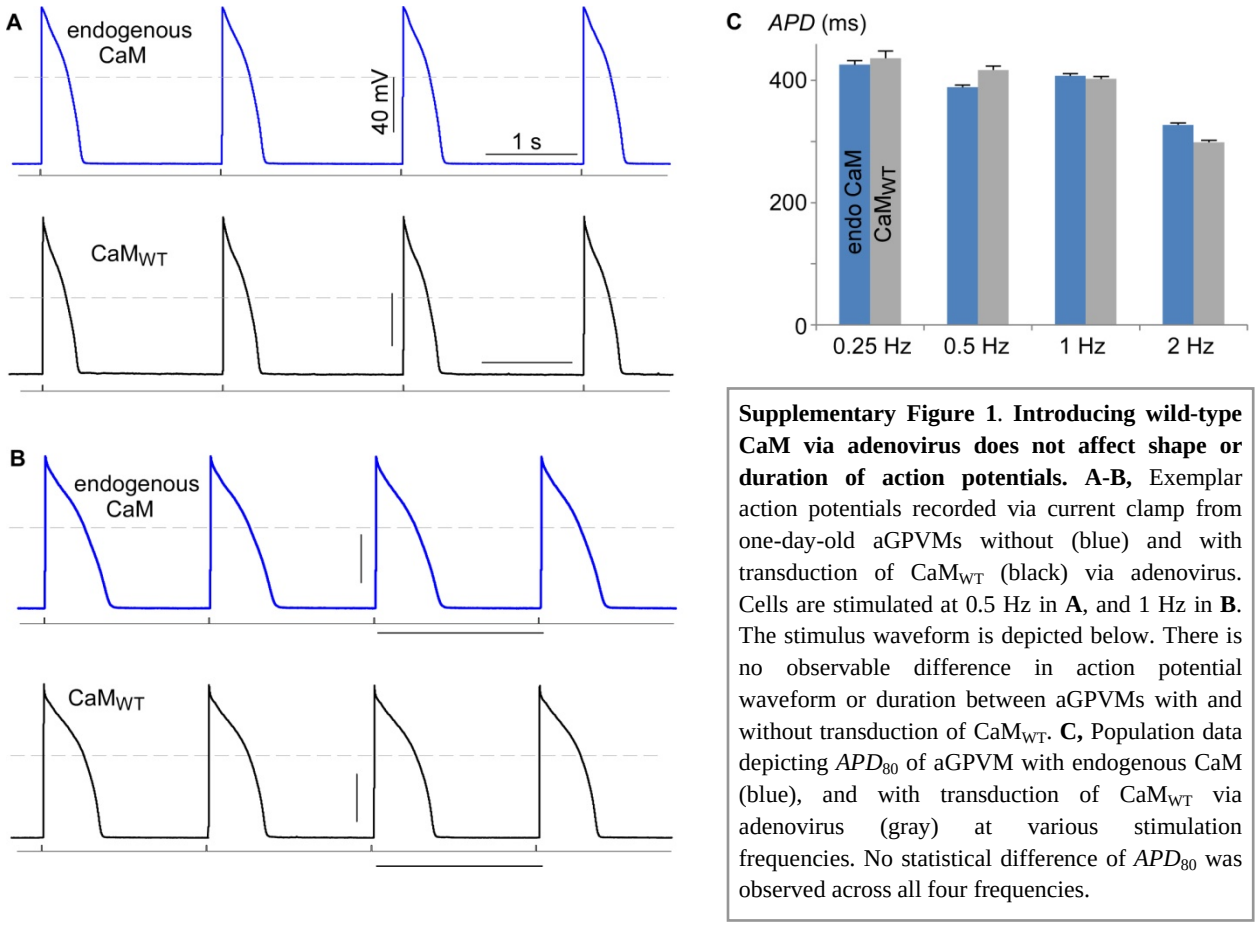

Supplementary Figure 1. Introducing wild-type CaM via adenovirus does not affect shape or duration of action potentials. A-B, Exemplar action potentials recorded via current clamp from one-day-old aGPVMs without (blue) and with transduction of CaM_{WT} (black) via adenovirus. Cells are stimulated at 0.5 Hz in **A**, and 1 Hz in **B**. The stimulus waveform is depicted below. There is no observable difference in action potential waveform or duration between aGPVMs with and without transduction of CaM_{WT}. **C,** Population data depicting APD_{80} of aGPVM with endogenous CaM (blue), and with transduction of CaM_{WT} via adenovirus (gray) at various stimulation frequencies. No statistical difference of APD_{80} was observed across all four frequencies.

1.2 CaM mutants produce similar effects at an alternate pacing rate.

To confirm our findings that LQTS CaM mutants can recapitulate the long-QT phenotypes at more than a single pacing rate, we also recorded action potential waveforms at faster pacing frequencies.

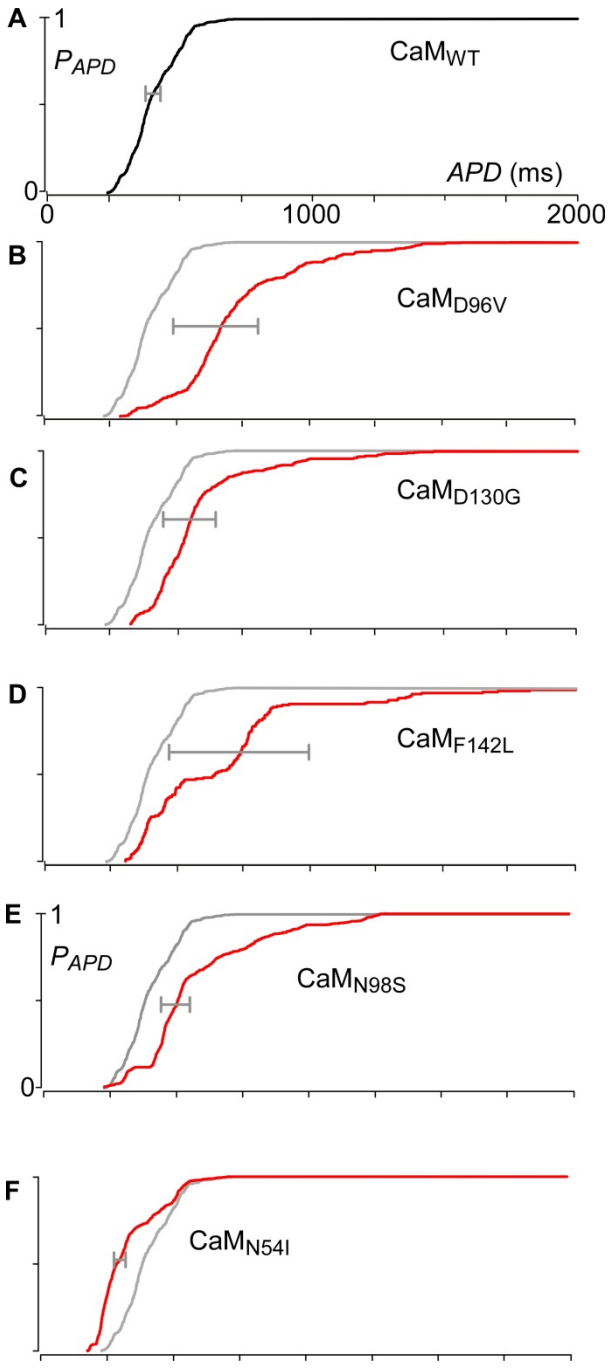

Supplementary Figure 2 shows the cumulative histograms of APD_{80}s for aGVPMs transduced with wild-type and mutant CaMs (as labeled) and paced at 1 Hz. Here, we observe the similar trend as compared to the 0.5 Hz pacing rate from the main text (Figures 1 and 3). Both action potential prolongation and increased APD dispersion are evident at the faster pacing rate.

Supplementary Figure 2. LQTS CaM mutants consistently prolong APD and increase heterogeneity during pacing at 1 Hz.
A, Population data of APD_{80} from one-day-old aGPVMs expressing CaM_{WT} stimulated at 1 Hz, shown as a cumulative histogram (black). Horizontal gray bars depict averaged standard deviation of APD_{80} within the same cells (SD_{cell}), here and throughout. 547 APs from n = 12 cells.
B, Cumulative histogram of APD_{80} from aGPVMs expressing CaM_{D96V} stimulated at 1 Hz (red) demonstrates a dramatic increase in APD_{80} (P < 0.01), consistent with data from aGPVMs stimulated at 0.5 Hz (Figure 1D). Cumulative histogram from aGPVMs expressing CaM_{WT} is shown here in gray for reference. Moreover, the CaM_{D96V} also significantly increases the heterogeneity of APD, shown here as a longer gray horizontal bar (SD_{cell}), compared to panel **A**. 526 APs from n = 9 cells.
C-D, CaM_{D130G} and CaM_{F142L} remarkably prolong APD and increase APD heterogeneity in aGPVMs stimulated at 1 Hz, consistent with data observed in aGPVMs stimulated at 0.5 Hz (Figures 1F and 1H). For D130G, 415 APs from n = 8 cells. For F142L, 172 APs from n = 4 cells.
E, The CPVT CaM mutant CaM_{N98S} also maintains its ability to increase APD at 1 Hz pacing. 724 APs from n = 7 cells.
F, CPVT CaM mutant N54I, on the other hand, has no effect on APD. 785 APs from n = 5 cells.

1.3 SR content and diastolic Ca^{2+}.

The increased Ca^{2+} load in the presence of LQTS CaM mutants is likely to effect the Ca^{2+} content of myocytes in several ways. Importantly, the sarcoplasmic reticulum (SR) is likely to take up some of the excess Ca^{2+} entry from slowly inactivating LTCCs, yielding a higher SR Ca^{2+} content. We tested this hypothesis by transducing aGPVMs with each LQTS CaM mutant and evaluating the SR Ca^{2+} content, gauged by undertaking Indo-1 imaging during emptying of SR Ca^{2+} by caffeine application (Supplementary Figure 3A). The result was a significantly larger SR Ca^{2+} content in the presence of LQTS CaM mutants, in agreement with the increase in Ca^{2+} transient amplitude seen in main text Figure 1. Moreover, expression of LQTS CaM mutants also significantly increased the diastolic Ca^{2+} level (Supplementary Figure 3B), measured after steady state pacing. Thus it appears that the marked increase in Ca^{2+} influx via LTCCs (due to diminished CDI), conspires with the resulting increased SR Ca^{2+} load, to produce large phasic Ca^{2+} transients during repetitive pacing.

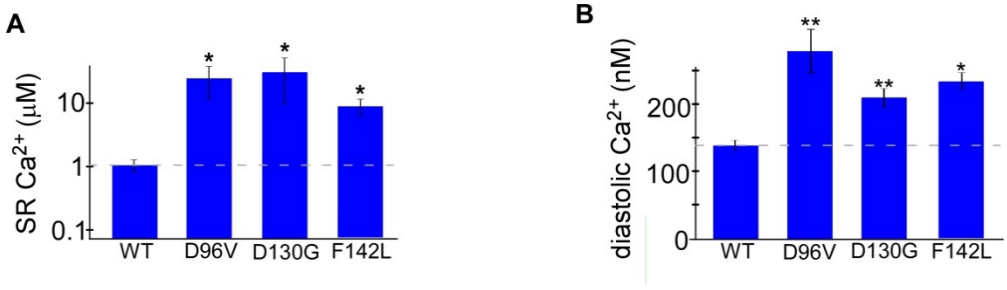

Supplementary Figure 3. SR Ca^{2+} load and diastolic Ca^{2+} concentrations.
A, SR Ca^{2+} content of aGPVMs transduced with LQTS CaM mutants is significantly higher than that of CaM_{WT} (*, $P < 0.01$, $n = 9, 3, 4$ and 4 cells, respectively). Load obtained after steady-state pacing.
B, Transduction of LQTS CaM mutants significantly increases the diastolic Ca^{2+} level of aGPVMs. Data obtained after steady-state pacing.(*, $P < 0.01$; ** $P < 0.05$, $n = 6, 15, 12, 18$ cells, respectively).

1.4 Summary of AP parameters for 1 Hz pacing.

To confirm phenotypes observed at 0.5 Hz pacing rate upon expression of LQTS and CPVT CaM mutants (Table 1 in the main text), we also recorded action potentials at other pacing rates. Supplementary Table 1 summarizes parameters from action potential recordings from 1 Hz pacing rate.

Supplementary Table 1: Average values for APs recorded during pacing at 1 Hz

CaM	APD_{80} (ms)	$(dV/dt)_{max}$ (mV/ms)	V_{rest} (mV)	V_{max} (mV)
WT	402.5 ± 4	104.5 ± 2	-63.7± 0.2	54.0 ± 0.3
D130G	567.5 ± 10*	112.2 ± 2	-63.7 ± 0.2	50.8 ± 0.7
D96V	720.2 ± 11*	100.3 ± 2	-63.7 ± 0.2	57.6 ± 0.6
F142L	685.7 ± 31*	129.7 ± 6	-63.7 ± 0.3	50.6 ± 0.9
N54I	326.9 ± 4	119.4 ± 1	-65.27 ± 0.3	50.7 ± 0.2
N98S	580.2 ± 8.6*	170.2 ± 2	-63.2 ± 0.2	53.7 ± 0.2

Supplementary Table 1. **Detailed parameters from action potential recordings.**
Besides large increase in APD_{80} upon expression of LQTS and CPVT CaM mutants, there was no statistically significant change in $(dV/dt)_{max}$ (maximum upstroke velocity), V_{rest} (resting membrane potential), or V_{max} (maximum membrane potential), as measured in aGPVMs expressing CaM mutants. (*, $P < 0.01$ versus WT).

1.5 Reduction of CDI due to LQTS CaM mutants under more physiological buffering conditions.

The data displayed in Figures 2-3 of the main text was obtained under high Ca^{2+} buffering conditions (10 mM BAPA). This high buffering condition limits Ca^{2+} elevations to within the local domain of Ca^{2+} channels, resulting in a component of Ca^{2+} regulation triggered predominantly by the C-lobe of CaM [1, 2]. This configuration was advantageous because CDI measures became independent of the level of channel expression, and the main effect of C-lobe CaM mutations was nicely observed in this arrangement. However, under more native Ca^{2+} buffering, a sustained global elevation of Ca^{2+} is present, which permits additional induction of a CDI component contributed by the N-lobe of CaM [1].

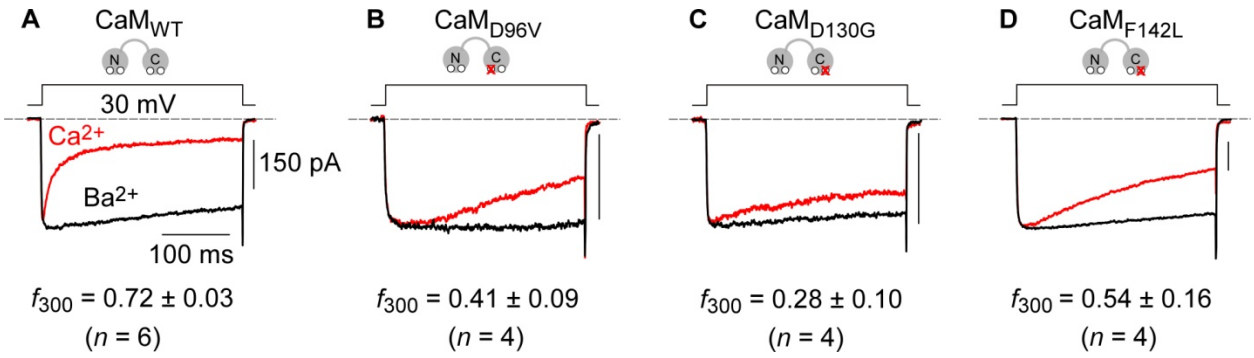

Supplementary Figure 4. **LQTS CaM mutants diminish CDI under modest Ca^{2+}-buffering. A,** Exemplar current traces recorded using 1 mM EGTA as intracellular Ca^{2+} buffer in HEK293 cells co-transfected with $Ca_V1.2$ and CaM_{WT}. Currents were evoked by a voltage step to 30 mV (top). Stronger decay in Ca^{2+} (red) current as compared to Ba^{2+} (black) represents CDI. Ba^{2+} current was scaled to the same magnitude as Ca^{2+} to facilitate comparison of decay kinetics, and the current scale bar pertains to Ca^{2+} here and throughout. f_{300}, representing the extent of CDI, is expressed as mean ± SEM here and throughout. **B,** Expression of CaM_{D96V} strongly blunts CDI, although to a smaller extent than in high Ca^{2+} buffering (10 mM BAPTA). **C-D,** Strong but incomplete blunting of CDI is also observed upon expression of CaM_{D130G} and CaM_{F142L}, respectively.

To assess the effects of CaM mutations under this more physiological buffering, we therefore obtained the equivalent whole-cell patch-clamp data (Supplementary Figures 4-5) under modest Ca^{2+} buffering (1 mM EGTA). Such conditions now allow for both local (C-lobe) and global (N-lobe) Ca^{2+}/CaM signaling. As the N-lobe remains unperturbed in the LQTS mutant CaMs, a small residual CDI due to N-lobe CaM regulation now emerges (Supplementary Figures 4B-D). Importantly, compared to CaM_{WT}, each of the LQTS CaM mutants demonstrate a dramatic reduction in CDI, validating the overall results under high buffering condition. Conversely, neither of the CPVT CaM mutants have a large

enough effect on CDI for any deficit to be observed under the modest Ca^{2+} buffering condition (Supplementary Figure 5).

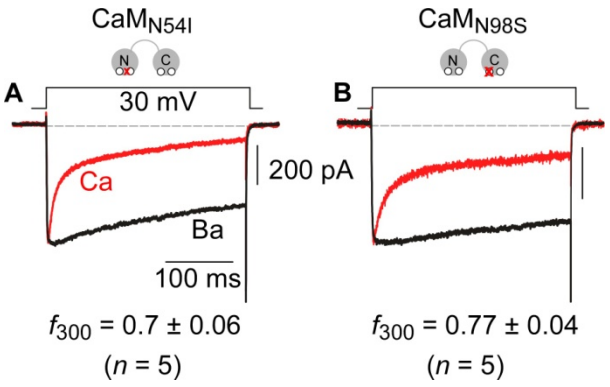

Supplementary Figure 5. CPVT mutants minimally affect CDI under modest Ca^{2+} buffering.
A, Full CDI is seen in the presence of CaM_{N54I}.
B, The small CDI deficit seen under high buffering conditions due to CaM_{N98S} is masked under modest internal Ca^{2+} buffering. Format is as in Supplementary Figure 4.

1.6 Calibrating the expression ratio of wild-type to mutant CaM

Before being able to accurately test the graded response of CDI at different expression ratios of wild-type to mutant CaM, we first needed to devise a method to control and validate the protein expression ratio relative to a transfected cDNA ratio. Through a simplistic yet powerful imaging method, we were able to determine a scaling factor *m* that relates the protein expression ratio ($\hat{\gamma}$) to cDNA transfection ratio (γ) as

$$\hat{\gamma} = m \cdot \gamma \tag{1}$$

First, we assessed the relative brightness of venus- and cerulean-tagged CaM_{WT} (V-CaM_{WT} and C-CaM_{WT}, in Supplementary Figure 6A). An equimolar ratio of cDNAs encoding these moities was transfected into HEK293 cells, and cell-by-cell epifluorescence imaging undertaken 1-2 days thereafter. Under these conditions, cells should on average express equal amounts of V-CaM_{WT} and C-CaM_{WT}. Indeed, this outcome is experimentally verified by: (a) the close adherence of cell-by-cell fluorescence measurements to a straight line, and (b) a slope (1/β) indistinguishable from the relative brightness of venus compared to cerulean (gauged from venus-cerulean dimer analysis, not shown). Indeed, if f_V is the venus fluorescence per molar concentration of venus in a HEK293 cells, and f_C the corresponding cerulean metric, then

$$1/\beta = f_V / f_C \tag{2}$$

Second, we accounted for potential differences in the expression of wild-type versus mutant CaM molecules, as elaborated from equimolar transfected cDNA. The approach is illustrated for the CaM_{D96V} mutant. Mixtures of V-CaM_{WT} and C-CaM_{D96V} were expressed, using different molar ratios of transfected DNA (γ). Supplementary Figure 6B displays cell-by-cell plots of whole-cell venus fluorescence ($F_{V\text{-}CaM/WT}$) versus corresponding cerulean fluorescence ($F_{C\text{-}CaM/D96V}$), where different-colored relations correspond to different cDNA transfection ratios γ, as labeled. The tight adherence of data points to corresponding linear relations confirms that each transfection ratio γ largely specifies a specific protein expression ratio ($\hat{\gamma}$), irrespective of total protein expression levels. Accordingly, the slope of each relation yields a value α, which relates to $\hat{\gamma}$ as

$$\alpha = \frac{F_{V\text{-}CaM/WT}}{F_{C\text{-}CaM/D96V}} = \frac{f_V[V-CaM_{WT}]}{f_C[C-CaM_{D96V}]} = \frac{f_V}{f_C} \cdot \frac{[V-CaM_{WT}]}{[C-CaM_{D96V}]} = \frac{1}{\beta} \cdot \hat{\gamma} \qquad (3)$$

where [V–CaM_{WT}] and [C–CaM_{D96V}] are the molar concentrations of the corresponding species in HEK293 cells. Thus, the protein expression ratio of CaM_{WT} to CaM_{96V} can be calculated as

$$\hat{\gamma} = \alpha \cdot \beta \qquad (4)$$

for each cDNA transfection ratio γ. Supplementary Figure 6C plots these entities ($\hat{\gamma} = \alpha \cdot \beta$ versus γ) against each other, furnishing a linear relationship whose slope yields the desired conversion factor *m* (= 0.98) for Equation 1. Thus, we could now specify the protein expression ratio of wild-type to mutant CaM ($\hat{\gamma}$) from cDNA ratios (γ) used for transfection.

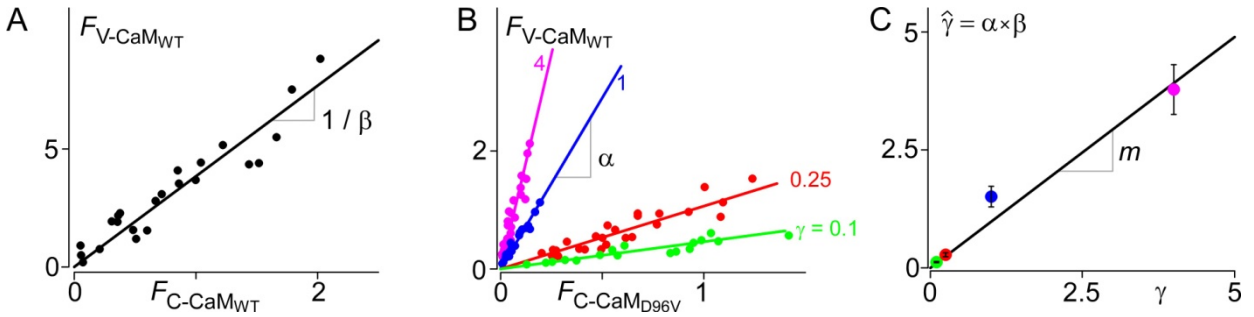

Supplementary Figure 6. Calibration of protein expression ratio between CaM_{WT} and CaM_{D96V}.
A, Cell-by-cell plot of venus versus cerulean fluorescence intensity, derived from venus- and cerulean-tagged CaM_{WT} (V-CaM_{WT} and C-CaM_{WT}), demonstrating a linear correlation with a slope of $1/\beta$.
B, Cell-by-cell plots of whole-cell venus fluorescence ($F_{V\text{-}CaM/WT}$) versus corresponding cerulean fluorescence ($F_{C\text{-}CaM/D96V}$) for various cDNA transfection ratios γ. Slopes of each relation specify α for each γ.
C, Plotting $\hat{\gamma}$ as a function of γ yields a linear relation with a slope equal to the final conversion factor *m*.

For the remaining two LQTS mutants, we confirmed that these mutations exhibit a similar *m* value, as follows. Holding γ = 1 (equimolar cDNA ratio of wild-type to mutant CaM) fixed for CaM_{D130G} and CaM_{F142L}, the resulting $\hat{\gamma}$ data points (colored symbols, Supplementary Figure 7) nicely superimpose on the $\hat{\gamma}$ versus γ relation for CaM_{D96V} (reproduced as black symbols and fit, from Supplementary Figure 6). Thus, we could use the same value of *m* throughout (~1).

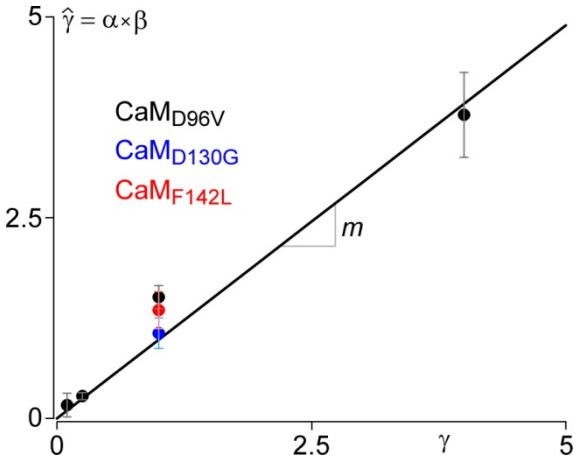

Supplementary Figure 7. Validation of conversion factor (*m*) for all CaM mutants.
The linear relationship between $\hat{\gamma}$ and γ of CaM_{D96V} (Supplementary Figure 6C) is reproduced here in black. The slope of this line is the conversion factor (*m*). The relationship between $\hat{\gamma}$ and γ for CaM_{D130G} (blue) and CaM_{F142L} (red) fall nicely along this same line, obtained from CaM_{D96V} (black). Thus, a similar conversion factor *m* ~1 may be utilized for all three CaM mutants.

1.7 Derivation of Langmuir CaM Ratio Equation

With careful calibrations of CaM protein expression in hand, we could quantify the graded CDI effects of the mutant CaMs. Since all three LQTS mutations are in the C-lobe of CaM, we continued to utilize high intracellular buffering (10 mM BAPTA) such that we need only consider C-lobe CaM regulation [1, 2] in our derivations. In addition, we have shown that the mutant apoCaMs can bind to the channels at least as well as the wild-type counterpart (Figures 5B-E). Therefore, at baseline, each channel will be in one of the first three configurations depicted in Supplementary Figure 8: empty (state 1); occupied by a wild-type apoCaM (state 2), or occupied by a mutant apoCaM (state 3). Furthermore, to minimize the effect of endogenous CaM, we strongly expressed a mixture of wild-type and mutant CaM molecules. Under this condition, essentially all channels will be occupied by apoCaM at rest, restricting occupancy to either state 2 or 3 at baseline. Upon a rise in intracellular Ca^{2+}, CaM_{WT} will bind Ca^{2+} and induce conformational changes which result in CDI (state 4). All LQTS CaM mutants, on the other hand, feature

disrupted Ca^{2+} binding sites in the C-terminal lobe, yielding a complete absence of CDI (Supplementary Figure 8, bottom, grayed out state 5).

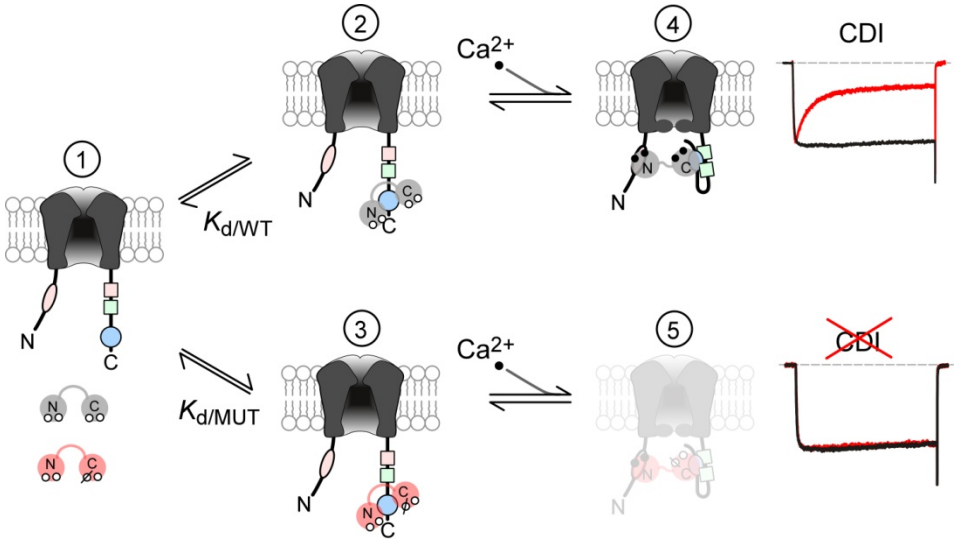

Supplementary Figure 8. **Model of CaM/channel interactions.**
Model depicting the configurations of CaM interacting with $Ca_V1.2$ channels. CaM_{WT} is depicted as the gray dumbbell-shaped molecule, and mutant CaM as the red dumbbell-shaped molecule. At low, resting Ca^{2+} levels, channels are either empty (state 1) or preassociated with either a wild-type apoCaM (state 2) or a mutant apoCaM (state 3). Upon a rise in intracellular, Ca^{2+} channels bound to a wild type CaM will transition from state 2 to state 4 upon Ca^{2+} binding to CaM, yielding CDI. Channels in state 3, however, are pre-bound to a mutant CaM which is unable to bind Ca^{2+} effectively. These channels are therefore unable to transition to state 5 and will thus lack CDI.

Since overexpression of LQTS CaM mutants produces *CDI* ~0 (in 10 mM BAPTA), the aggregate amount of CDI directly reflects fraction of channels in state 2 (f_2):

$$CDI = CDI_{WT} \cdot f_2 \tag{5}$$

At equilibrium, f_2 can be calculated as

$$\frac{f_2}{f_1} = \frac{C_{\mathrm{WT}}}{K_{\mathrm{d/WT}}} \text{ which gives } \quad f_2 = f_1 \cdot \frac{C_{\mathrm{WT}}}{K_{\mathrm{d/WT}}} \tag{6}$$

$$\frac{f_3}{f_1} = \frac{C_{\mathrm{MUT}}}{K_{\mathrm{d/MUT}}} \text{ which gives } \quad f_3 = f_1 \cdot \frac{C_{\mathrm{MUT}}}{K_{\mathrm{d/MUT}}} \tag{7}$$

where f_1 and f_3 represent fractions of channels in state 1 and 3, respectively; C_{WT} and C_{MUT} represent the concentration of wild-type and mutant CaM, respectively; and $K_{\mathrm{d/WT}}$ and $K_{\mathrm{d/MUT}}$ represent dissociation constants for wild-type or mutant CaM interaction with channels.

At baseline (before elevation of Ca^{2+}), we have that

$$f_1 + f_2 + f_3 = 1 \tag{8}$$

such that, we can combine Equations 6, 7 and 8 to obtain

$$f_1 \cdot (1 + \frac{C_{\mathrm{WT}}}{K_{\mathrm{d/WT}}} + \frac{C_{\mathrm{MUT}}}{K_{\mathrm{d/MUT}}}) = f_1 \cdot D = 1 \tag{9}$$

Since we strongly overexpressed wild-type and mutant CaM, C_{WT} and C_{MUT}, which yields

$$\lim_{C_{\mathrm{WT}},\, C_{\mathrm{MUT}} \to \infty} D = \frac{C_{\mathrm{WT}}}{K_{\mathrm{d/WT}}} + \frac{C_{\mathrm{MUT}}}{K_{\mathrm{d/MUT}}} \tag{10}$$

Hence,

$$f_2 = f_1 \cdot \frac{C_{\mathrm{WT}}}{K_{\mathrm{d/WT}}} = \frac{1}{D} \cdot \frac{C_{\mathrm{WT}}}{K_{\mathrm{d/WT}}} = \frac{C_{\mathrm{WT}} / C_{\mathrm{MUT}}}{K_{\mathrm{d/WT}} / K_{\mathrm{d/MUT}} + C_{\mathrm{WT}} / C_{\mathrm{MUT}}} = \frac{\hat{\gamma}}{K_{\mathrm{d/WT}} / K_{\mathrm{d/MUT}} + \hat{\gamma}} \tag{11}$$

finally, yielding aggregate CDI as

$$CDI = CDI_{WT} \cdot \frac{\hat{\gamma}}{K_{d/WT} / K_{d/MUT} + \hat{\gamma}} \text{ or } \frac{CDI}{CDI_{WT}} = \frac{\hat{\gamma}}{\Lambda + \hat{\gamma}} \tag{12}$$

where $\Lambda = K_{d/WT} / K_{d/MUT}$.

1.8 Dose-Dependent Effect of CaM_{D130G} and CaM_{F142L}

In Figure 6 of the main text, we focused on the graded effects of variable expression ratios of CaM_{WT} to CaM_{D96V}. Here, we show that the mutants CaM_{D130G} and CaM_{F142L} also result in similar graded reductions of CDI (Supplementary Figure 9). Because of the preassociation of apoCaM and Ca^{2+} channels [3, 4], and the fact that mutant apoCaM can bind to the channels at least as well as the wild-type apoCaM (Figures 5D-E), the CDI dose response to the relative protein expression ratio of wild-type and mutant CaMs ($\hat{\gamma}$) follows the Langmuir predictioin (Equation 12) precisely for all three LQTS mutant CaMs.

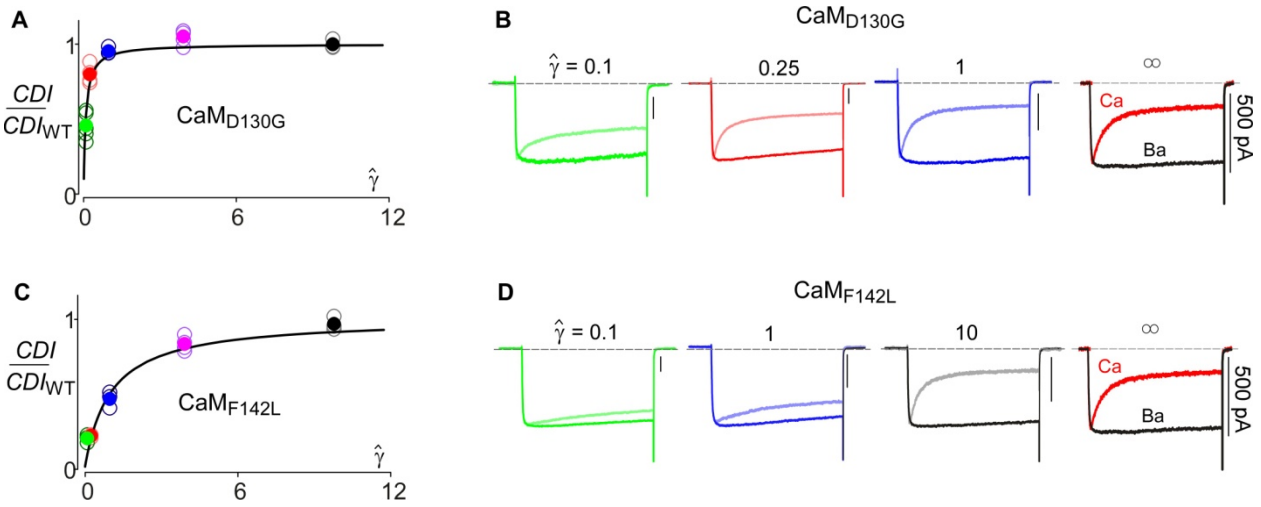

Supplementary Figure 9. **Dose-dependent effect of CaM_{D130G} and CaM_{F142L}.**

A, Langmuir plot of normalized *CDI* as a function of $\hat{\gamma}$, ratio of protein expression levels of CaM_{WT} and CaM_{D130G}. Solid circles indicate average data for each ratio $\hat{\gamma}$; open circles are data from individual cells. Black curve drawn with $\Lambda \sim 0.1$.

B, Exemplar current traces corresponding to the data in panel **A** with the similar color code for each value of $\hat{\gamma}$. For each, the Ca^{2+} trace is the lighter color, with the corresponding Ba^{2+} trace normalized to the peak of the Ca^{2+} trace for comparison. Scale bar corresponds to Ca^{2+}. Exemplar current traces from cells expressing CaM_{WT} only ($\hat{\gamma} = \infty$) is reproduced from Figure 2A for reference.

C, Langmuir plot of normalized *CDI* as a function of $\hat{\gamma}$, ratio of protein expression levels of CaM_{WT} and CaM_{F142L} in a similar format as **A**. Black curve drawn with $\Lambda \sim 1$.

D, Exemplar current traces corresponding to the data in **C**. Same format as **B**.

2. Supplementary Movies

Supplementary Movie 2.1. Action-potential recording from a single ventricular myocyte transduced with CaM_{WT} corresponding to main text Figure 1A. The action potentials are stimulated at a frequency of 0.5 Hz and demonstrate a regular rhythm.

Supplementary Movie 2.2. Action-potential recording from a single ventricular myocyte transduced with CaM_{D96V} corresponding to main text Figure 1C. The action potentials are stimulated at a frequency of 0.5 Hz and display severe prolongation of the action potential consistent with LQTS.

Supplementary Movie 2.3. Action-potential recording from a single ventricular myocyte transduced with CaM_{D130G} corresponding to main text Figure 1E. The action potentials are stimulated at a frequency of 1 Hz and exhibit alternans.

Supplementary Movie 2.4. Action-potential recording from a single ventricular myocyte transduced with CaM_{F142L} corresponding to main text Figure 1G. The action potentials are stimulated at a frequency of 1 Hz and display another example of severe prolongation of the action potential at a different pacing rate from Supplementary Movie 2.2.

3. References

[1] Dick IE, Tadross MR, Liang H, Tay LH, Yang W, Yue DT. A modular switch for spatial Ca2+ selectivity in the calmodulin regulation of CaV channels. Nature. 2008;451:830-4.

[2] Tadross MR, Dick IE, Yue DT. Mechanism of local and global Ca2+ sensing by calmodulin in complex with a Ca2+ channel. Cell. 2008;133:1228-40.

[3] Erickson MG, Alseikhan BA, Peterson BZ, Yue DT. Preassociation of calmodulin with voltage-gated Ca(2+) channels revealed by FRET in single living cells. Neuron. 2001;31:973-85.

[4] Zuhlke RD, Pitt GS, Deisseroth K, Tsien RW, Reuter H. Calmodulin supports both inactivation and facilitation of L-type calcium channels. Nature. 1999;399:159-62.